Utrecht University

Master Thesis

$CoCu/SiO_2$ catalysts via galvanic replacement for CO hydrogenation to higher alcohols

Debye Institute for Nanomaterials Science

Inorganic Chemistry and Catalysis

Utrecht University

Daily supervisor: R. (Remco) Dalebout, MSc
Project supervisor: prof. dr. P.E. (Petra) de Jongh
Second examiner: dr. B. (Baira) Donoeva

W. (Willem) Eijsvogel, BSc

March 7, 2019

Abstract

Higher alcohols can be synthesized from syngas (CO/H_2) with a CuCo catalyst, however no catalyst was sufficient in performance and reproducibility to reach past the pilot plant stage. A criterion for improving the selectivity towards higher alcohols is the intimacy between both metals, which can be attained with galvanic replacement. In this work, the synthesis of CuCo catalysts *via* galvanic replacement of pre-deposited Co nanoparticles on SiO_2 by Cu ions is investigated to gain better understanding and control over the Cu deposition. Various Cu precursors and solvents were used to determine their effects on the galvanic replacement reaction. Use of organic solvents for galvanic replacement yielded low Cu deposition and leaching of Co as determined by ICP. Galvanic replacement with aqueous Cu^{2+} solutions yielded excellent Cu deposition and is the most promising for catalyst synthesis, however irreducible Co silicates were formed rendering this catalyst inactive. The intimacy between Cu and Co was determined with (S)TEM-EDX and XRD. The catalytic performance and stability of each catalyst was evaluated in the CO hydrogenation reaction. The higher alcohol selectivity of the active catalysts was up to 6%, however primarily hydrocarbons were formed (around 90%). The catalysts synthesized via galvanic replacement showed a notably lower selectivity towards methanol compared to a catalyst prepared *via* conventional co-impregnation, suggesting a better metal intimacy. This work presents a step forward towards a better higher alcohol synthesis catalyst, however the next challenge that needs to be addressed is the formation of Co silicates when aqueous solutions are used.

Contents

1 Introduction

Higher alcohols (HA), defined as alcohols with two or more C atoms, have many applications in both the energy sector and chemical industries. In the energy sector they are for instance used as fuel additives to increase the octane number of gasoline and thus efficiency, and in chemical industries as chemical building blocks for products such as butadiene or as solvents.[1] Currently, ethanol is mainly produced by sugar fermentation and hydration of ethylene. For other higher alcohols the latter process is also used but with their corresponding alkene instead.[2,3] Another way to produce higher alcohols would be direct conversion from syngas (H_2/CO), which would have the economic advantage of requiring less energy to isolate the product than e.g. sugar/starch fermentation[4] and the potential environmental benefit as syngas can be made from biomass rather than fossil fuels. However, such plants never made it past the pilot stage as catalyst performance (selectivity and activity) was either insufficient or the catalyst would be too expensive due to use of scarce metals such as Rh, limiting economic feasibility.[5,6]

For the direct conversion of syngas to alcohols, there are several different families or categories of catalysts. These are 1) Mo-based, 2) Rh-based, 3) modified Fischer-Tropsch (CuFe and CuCo based) and 4) modified methanol synthesis (Cu/ZnO based) catalysts. Each family has different advantages and disadvantages regarding selectivity, stability, cost, *etc.*. An overview of HAS catalysts from the four families and their catalytic performance is depicted in Figure 1.

Rh-based catalysts have been widely researched due to the unique electronic properties of Rh, as it is located between the CO-dissociating (*e.g.* Co and Fe) and non-CO-dissociating elements (*e.g.* Pd and Pt).[7] This type of catalysts is characterized by a high ethanol selectivity, but barely any of the more valuable C_{3+} alcohols.[8] The selectivity primarily towards ethanol combined with the high cost of Rh (€81.000/kg[9]) and lower conversion compared to the other HAS catalyst families all make it more challenging for this type to reach commercialization.[2]

Mo-based catalysts can be divided into four separate categories as well, with either MoS_2, MoO_x, Mo_2C or MoP as the active phase. They have a remarkable resistance to sulphur poisoning.[10] In order to boost the relatively low activity of Mo-based catalysts, these catalysts are promoted with transition metals as Co, Ni and Fe (common elements for Fischer-Tropsch synthesis).[2,10] Furthermore, they require promotion by an alkali metal (typically K) as well in order to shift the product selectivity from hydrocarbons to alcohols, however the hydrocarbon selectivity remains problematic.

It has been noted almost a century ago that methanol synthesis catalysts also produced some C_2-C_4 alcohols when they still contained alkali metal impurities after being synthesized.[11,12] The role of these alkali metal promotors is believed to be due to the basicity of these metals, inhibiting the side reactions by neutralising acidic sites and boosting C-O and C-C coupling by providing basic sites. However, this improved selectivity comes at the cost of a lower catalyst activity.[13] Typical modified methanol synthesis catalysts consist of Cu/ZnO/Al_2O_3, Cu/ZnO/Cr_2O_3 or Cu/ZnO/ZrO_2, promoted with alkali metals and transition metals such as Co, Ni and Fe but also Mn and Mo. The main products of these catalysts are shorter alcohols, such as methanol, ethanol, propanol and (iso-)butanol.[13]

Modified Fischer-Tropsch (FT) catalysts consist primarily of either CuCo- or CuFe-based catalysts, derived from typical Co and Fe FT catalysts as the name suggests. The first patents for M-FT catalysts were granted around 1980 to Institut Français du Pétrole (IFP), based on Co and Cu as main components and up to three additional transition and alkali metal promotors.[14,15] The original patent claims alcohol selectivities of up to 95%, however contemporary papers had issues reproducing these

results. It was noted that the homogeneous distribution of active sites was critical, as minor changes in catalyst preparation could severely affect performance (*e.g.* due to agglomerations of one type of active site or separation from different types of active sites).[16] Due to the relatively good HA yield (Figure 1) combined with the low material costs (Co:€29.19/kg[9], Cu:€5.72/kg[9]), m-FTS catalysts have been the most extensively researched HAS catalysts in both academia and industry. Of these, CuCo-based catalysts have been researched the most of m-FTS catalysts. A lot of this research has been dedicated to the synthesis, as the system can be very finicky. For instance, the conversion during CO hydrogenation can vary a lot simply by changing precursors of both the main components and the promotors, as shown by the work of Matsuzaki *et al.*.[17] Even with novel synthesis methods such as nanocasting[18] or a colloidal synthesis route[19], catalyst performance has not been sufficient thus far.

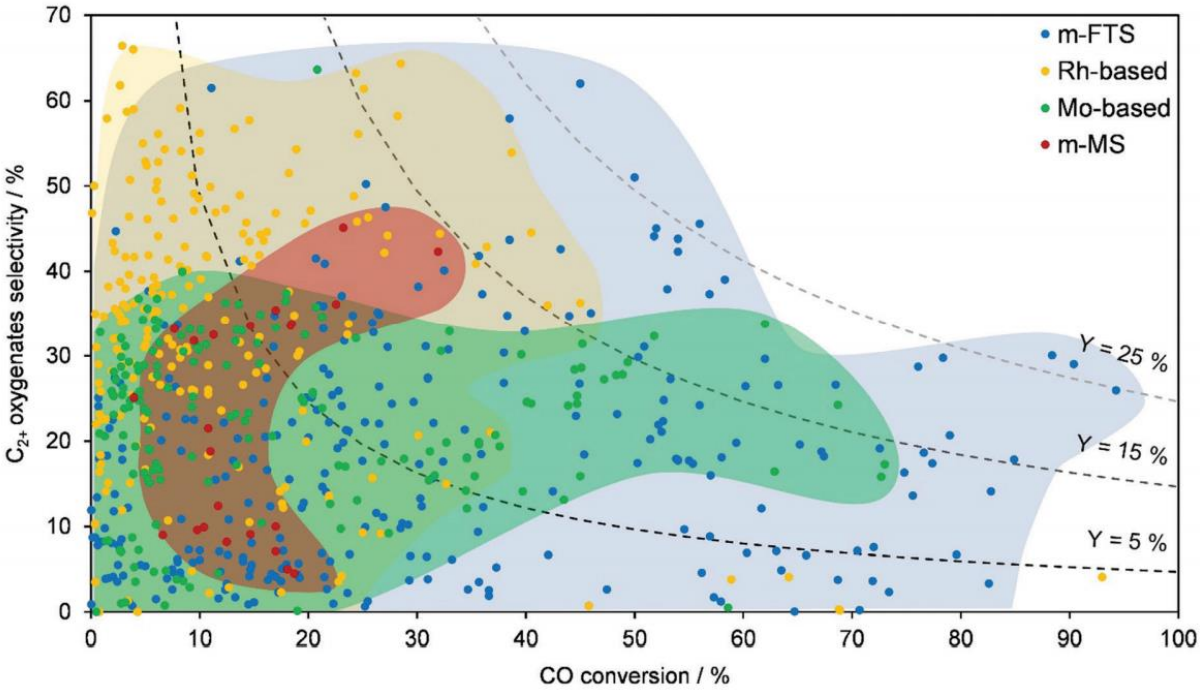

Figure 1 – HAS catalyst performances from all the papers reviewed by Luk *et al.*[2], showing the C_{2+} oxygenate selectivity against the CO conversion for all four main HAS catalyst families. Modified Fischer-Tropsch (m-FTS) catalysts are given in blue, Rh-based in yellow, Mo-based in green and modified methanol synthesis (m-MS) is given in red. The dashed lines represent the yield (Y) of 25%, 15% and 5% respectively. Figure reproduced from Ref[2].

Proximity between Co and Cu metal sites has often been cited as crucial for higher alcohol formation.[20–22] In order to achieve this intimacy, synthesis *via* galvanic replacement (GR) shows much potential. Galvanic replacement is a redox process where a metal is replaced by a more noble metal ion, which can be used for the synthesis of bimetallic particles.[23–25] Nafria *et al.*[19] synthesized CuCo core-shell nanoparticles by first synthesizing colloidal Co particles and subsequently forming a Cu shell around the particles *via* galvanic replacement. The core-shell nanoparticles were then deposited on a SiO_2 support and characterized after heat treatment, causing NP growth due to formation of an oxide layer. Next, the catalyst was reduced which caused NP shrinkage and inversion of core and shell. The catalyst was then used in CO_2 hydrogenation where the core-shell particles transformed into two separate, but touching, metallic domains. During the work for this thesis, a paper based on the same premise but applied to a different system and reaction was published, namely bimetallic Ru-M on TiO_2 (where M = Fe, Cu, Co and Ni) for the selective hydrogenation of benzene.[26] In the work of Zhou *et al.*, the metal M was first deposited *via* wetness impregnation and then chemically reduced with $NaBH_4$. After reduction, the bimetallic particles were made by galvanic replacement followed by an acid treatment

to tune the content of metal M. The work of Zhou *et al*. shows the viability of galvanic replacement of supported metal nanoparticles to create bimetallic particles.

In earlier work performed in this group, based on the work of Nafria *et al*., CoCu core-shell nanoparticles supported on SiO_2 were synthesized using galvanic replacement on pre-deposited Co particles.[27] They first made small (around 3 to 5 nm), well dispersed Co nanoparticles on SiO_2. The Cu was then deposited by adding a Cu solution (either CuCl or CuOAc) in oleylamine to a suspension of the supported Co NPs in dichlorobenzene, all under inert atmosphere. This lead to a good intimacy between both metals, however the galvanic replacement reaction consistently did not take place to the expected extent. This lead to a lower-than-aimed-for loading of Cu. They noted that changing the precursor from CuCl to CuOAc slightly increased copper deposition, as well as increasing the reaction temperature during galvanic replacement.

In this research the synthesis of a m-FTS catalyst *via* galvanic replacement, specifically a CuCo catalyst supported by SiO_2, is further investigated. First, metallic Co nanoparticles on SiO_2 were prepared with incipient wetness impregnation followed by calcination and reduction. Next, galvanic replacement was performed to deposit Cu on the catalyst. In order to improve the Cu deposition compared to our earlier work, various Cu precursors and solvents were used for the reaction. The catalysts were primarily characterized with XRD, (S)TEM-EDX, and ICP. Furthermore, the stability and selectivity towards higher alcohols of the synthesized $CuCo/SiO_2$ catalysts in the CO hydrogenation reaction were tested. It was found that especially solvent plays a significant role in the galvanic replacement of supported Co nanoparticles with Cu.

2 Theory

2.1 Reaction pathway towards higher alcohols

Both Cu and Co (oxides) are active for CO hydrogenation reactions. Cobalt is widely used for Fischer-Tropsch (FT) catalysts for CO hydrogenation to synthesize hydrocarbons, this process starts with the dissociative adsorption of CO on Co followed by carbon chain growth via C-C coupling. Bezemer *et al.*[28] have shown that the optimal Co particle size for FT is around 6-8 nm, as smaller particles would lead to a sharp drop in the turnover frequency (TOF) while larger particles lead to less active sites per weight due to a decreased surface area. The authors proposed that a minimum Co particle size is required to stabilize the monoatomic step sites that act as stable FT sites.[28] Supported Cu/ZnO on the other hand is used for CO hydrogenation to methanol, which begins with associative adsorption of CO. The activity scales roughly linear with copper surface area for this reaction, which means smaller particles are preferred.[29] Current work done in our group on CuCo catalysts shows that for small particles of around 3 nm, methane is the dominant product. This is in line with Co FT catalysts, where smaller (<5 nm) lead to a sharp increase in methane selectivity.[28]

Higher alcohol synthesis (HAS) with CuCo catalysts is proposed to take place via a dual site mechanism, making use of the different CO adsorption properties of Co and Cu to adsorb CO dissociatively and associatively respectively (Figure 2). However, some research also suggests that Co/Co^{n+} species perform both functions of the dual site mechanism.[30,31]

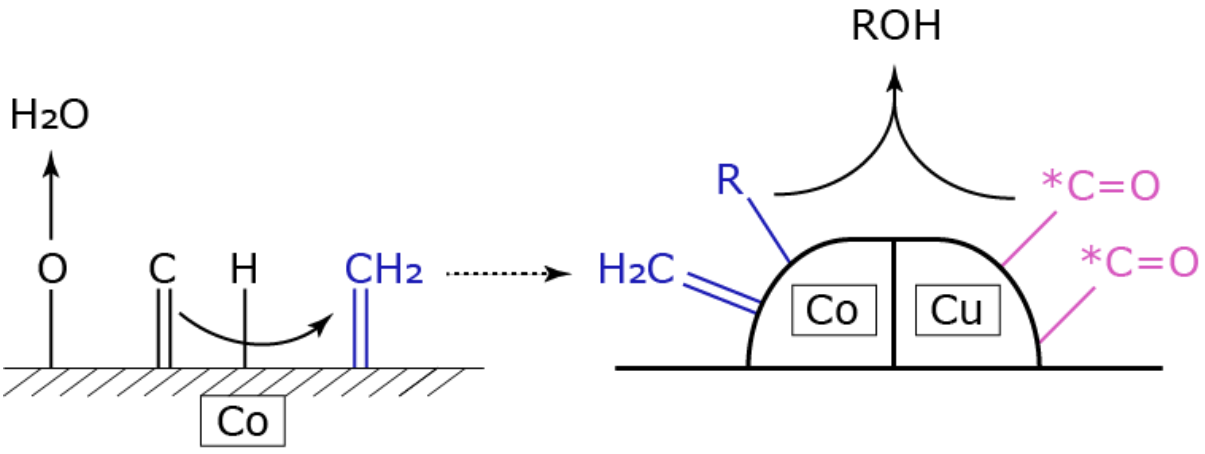

Figure 2 – Depiction of the basic principle behind the dual site mechanism for higher alcohol synthesis of a CuCo-based catalyst. On the left, CO is adsorbed dissociatively on the cobalt surface and subsequently hydrogenated. On the right, CO is shown to adsorb associatively on Cu, which is then incorporated in the growing carbon chain R to yield alcohols. Image reproduced from the work of Xiao K. *et al.*[22].

Figure 3 shows the reaction scheme for the production of higher alcohols and hydrocarbons from syngas, ignoring other side reactions. The scheme starts with CO which is adsorbed either associatively (1a), which can be hydrogenated to produce methanol directly, or dissociatively (1b); the former primarily takes place on Cu surfaces while the latter takes place on Co surfaces. After hydrogenation of C* (2) to C_1H_x* (where 1 < x < 4), there are three possibilities: insertion of CO* to yield an alcohol (2a), complete hydrogenation to yield a hydrocarbon (2b), or C-C chain growth via CH_x* addition. This highlights importance of the proximity between Cu and Co sites for higher alcohol synthesis as dissociative adsorption requires Co while the CO* insertion requires Cu; both are required to synthesize higher alcohols.[22] The product ratio of hydrocarbons and higher alcohols depends on the partial CO pressure, the dissociation rate and the hydrogenation rate according to Xiaoding *et al.*[16], of

which the latter two are catalyst dependent. Prieto et al. determined that a Cu/Co atomic ratio of 0.33/0.66 is optimal for alloyed particles for HAS[20].

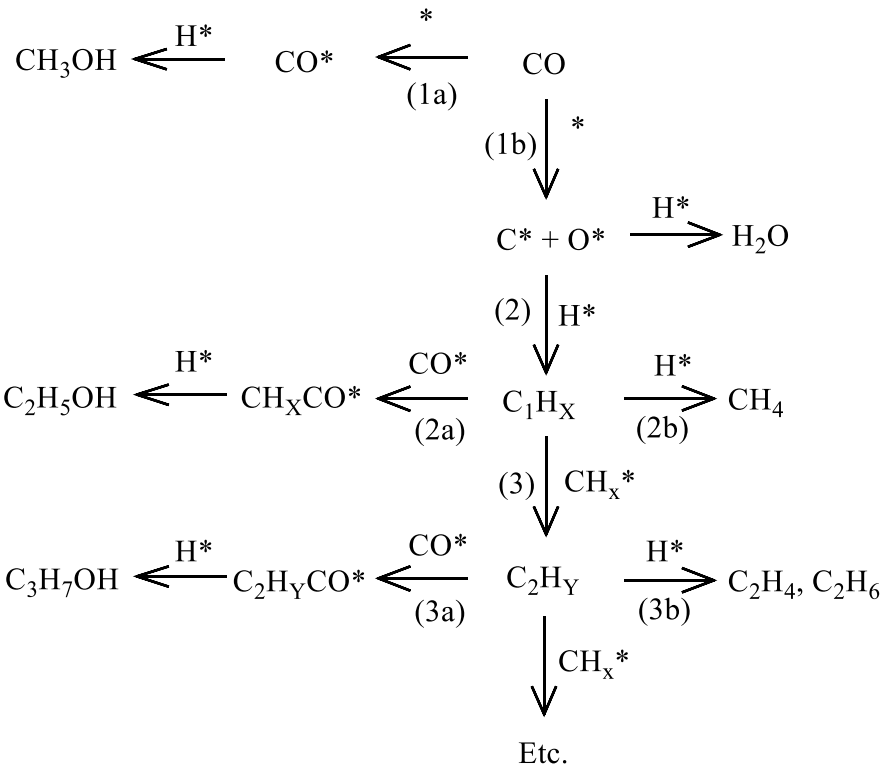

Figure 3 - Scheme for the production of higher alcohols from syngas. Adsorption sites and adsorbed species are indicated with an asterisk (*). Image adapted from [16].

2.2 Associative vs. Dissociative adsorption of CO

The CoCu bimetallic catalyst relies on the dissociative adsorption of CO on Co and the associative adsorption on Cu. The cause of the different adsorption behavior is explained as follows. When a molecule approaches the surface of a d-block metal, the energy levels of bonding and antibonding orbitals of the adsorbate will be broadened and shifted to lower energies due to interaction with the sp-band. The interaction of the d-band with the adsorbate energy levels will cause them to split into a pair of bonding and antibonding (towards the metal-adsorbate bond) chemisorption orbitals, which is shown in Figure 4 using the simple example of H_2. If electrons fill the orbitals derived from σ*, the internal molecular bond will be weakened which may lead to dissociation (of CO). Note that despite weakening the bond in the molecule, the interaction strength with the surface still increases. The phenomenon of the filling of the antibonding orbital by the electrons of the d-band from the metal is called 'back donation'.[32]

For the interaction of CO with transition metals such as Cu and Co, the chemisorption energy is dominated by the interaction of the antibonding orbital (σ*) with the d band. A more filled d band leads to lower energy level of the centre of the band. This is unfavorable for stronger interaction between the metal and CO, and leads to a higher energy barrier for dissociative adsorption. From the Cu electron configuration of $[Ar]3d^{10}4s^1$ and Co $[Ar]3d^7 4s^2$ configuration, it follows that CO dissociates more readily on Co. This difference in associative/dissociative adsorption leads to different reaction products in CO hydrogenation, e.g. methanol for Cu and hydrocarbons for Co.

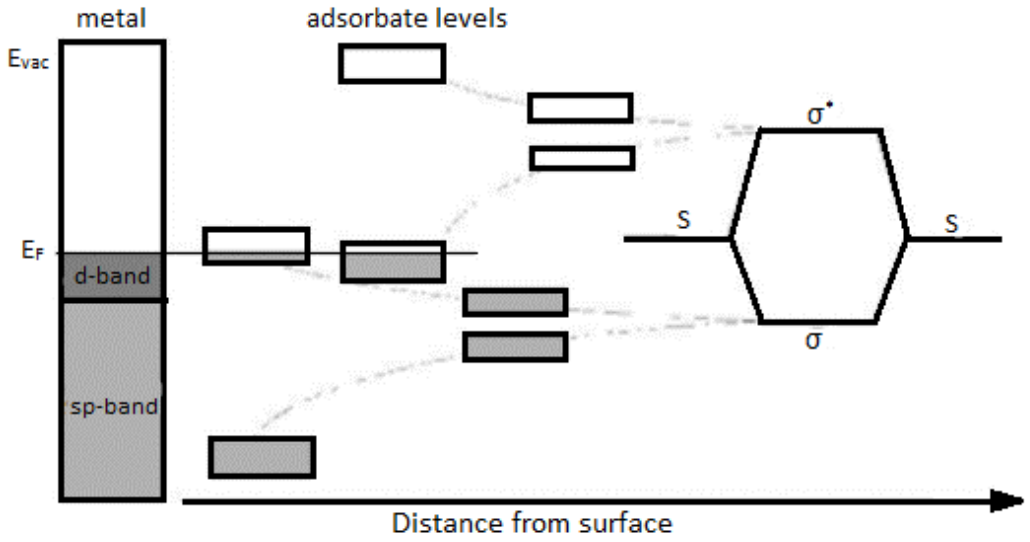

Figure 4- A molecule with a bonding σ and antibonding orbitals σ interacts with both the sp band and the narrow d band of the transition metal.*[32]

2.3 Galvanic Replacement

Galvanic replacement is an electroless deposition (*i.e.* without the use of an external current) technique that involves a less noble metal M_1 (the so-called 'sacrificial template') being immersed into a solution of a more noble metal M_2 which leads to M_2 replacing M_1 via an oxidation-reduction (redox) reaction. Galvanic replacement is frequently used in the synthesis of (bi)metallic nanostructures, *e.g.* hollow nanocubes, core-shell or nanorods. This is used because it allows for good control over composition, shape and morphology of the nanoparticles while remaining experimentally simple.[33] The size and shape can be altered based on the initial morphology of the sacrificial template and the ratio between reactants. In literature, most research performed is based on Ag colloids as a sacrificial template, despite the applicability of the technique on basically any metals with suitable redox potentials. This is because the chemistry of colloidal silver is broad and well-explored.[34] The second metal is typically a noble metal like Pt, Pd or Au to either partially or completely replace the sacrificial template, resulting in hollow or alloyed structures.[33]

Galvanic replacement can be used on metal nanoparticles deposited on a support as well,[26,35,36] though this is rarely reported in literature. This is likely due to the superior size and shape control given by colloidal synthesis so full advantage can be taken of the galvanic replacement reaction, and if desired, the colloids can be deposited onto a support afterwards. While a technique like incipient wetness impregnation does not yield the same level of control compared to colloidal synthesis over the sacrificial template, it is cheap, facile and thus widely used both in academia and industry.

As mentioned above, galvanic replacement is a redox reaction between a metal atom and metal ion with the difference in the standard electrode potential as the driving force behind the reaction.[24,25] The general redox half reactions between metals M_1 and M_2 is as follows:

$$(1)\ M_1^0 \rightarrow M_1^{z_1+} + z_1 e^-$$

$$(2)\ M_2^{z_2+} + z_2 e^- \rightarrow M_2^0$$

(1) and (2) together give:

$$(3)\ M_2^{z_2+} + (z_2/z_1)\ M_1^0 \rightarrow M_2^0 + (z_2/z_1)\ M_1^{z_1+}$$

with z_i the amount of exchanged electrons of metal *i*.

The driving force of this reaction comes from the difference in the standard electrode potential E°, according to the formula

$$(4)\ \Delta G° = -zF\Delta E°$$

where the reaction is spontaneous if

$$(5)\ \Delta G° < 0$$

with ΔG° as the change in Gibbs free energy, *z* the amount of exchanged electrons and F the Faraday constant. Following this, ΔE° > 0 must be the case for the reaction to take place.

The stoichiometric ratio (z_2/z_1) between the two metals is important for the final structure after galvanic replacement. A common literature example is between $AuCl_4^-$ and Ag: 3 Ag atoms are oxidized per Au atom deposited, leading to hollowed-out nanoparticles.[23] By reversing the stoichiometric ratio, (*e.g.* Cu and Ag^+ where 2 Ag atoms are deposited per Cu oxidized) an expanded core-shell structure is expected upon (partial) galvanic replacement.[23] Another aspect of galvanic replacement, though less relevant for this work, is the facet selectivity. The facets with the highest surface free energy are

replaced first, whereas if there is only one type of facet present the reaction will start somewhere random on the nanoparticle.[37,38]

Table 1 - Standard electrode potentials of relevant redox half reactions at 25°C and 1 atm.[39]

Redox half reaction	Standard electrode potential E° (V)
$Cu^{2+} + 2\ e^- \leftrightharpoons Cu$	0.34
$Cu^{+} + e^- \leftrightharpoons Cu$	0.52
$Co^{2+} + 2\ e^- \leftrightharpoons Co$	-0.28
$Co^{3+} + e^- \leftrightharpoons Co^{2+}$	1.92

In this work, galvanic replacement was used to partially replace Co nanoparticles on SiO_2 with Cu. The relevant half reactions and their standard electrode potentials are given in Table 1, and a depiction of the galvanic replacement with Cu^+ is shown in Figure 5. Both Cu^+ and Cu^{2+} were used as metal ions, which if inserted into equation (3) and (4) give:

$2\ Cu^+ + Co \rightarrow 2\ Cu + Co^{2+}$; $\Delta E° = 0.80$ V and $\Delta G° = -154.4$ kJ/mol.

$Cu^{2+} + Co \rightarrow Cu + Co^{2+}$; $\Delta E° = 0.62$ V and $\Delta G° = -119.7$ kJ/mol.

The above values are only valid for 'standard' (*i.e.* 25°C and 1 atm) conditions, however. Factors such as different ion concentrations, temperature or non-aqueous solutions will influence the reduction potential and thus the replacement reaction.[40]

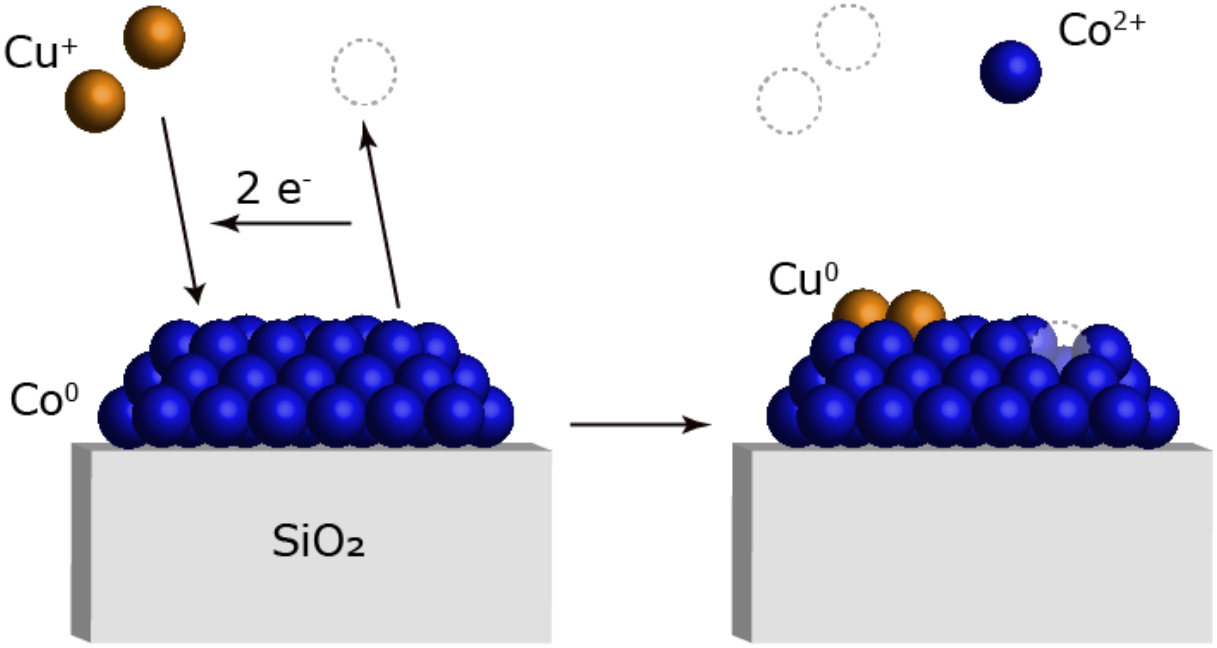

Figure 5 – The galvanic replacement reaction of Co^0 as a sacrificial template with Cu^+. Two Cu atoms are deposited per Co ion formed, until either all of the Co^0 or Cu^+ has reacted.

3 Experimental

3.1 Synthesis

3.1.1 Preparation of Co particles on SiO_2

All samples were prepared via incipient wetness impregnation (IWI). The Co precursor solution was made by dissolving 12.707g $Co(NO_3)_2 \cdot 6\ H_2O$ (Acros Organics, Cobalt(II) nitrate hexahydrate, 99+%) in 25 ml H_2O (Milli-Q). To ensure a more homogeneous concentration distribution inside the SiO_2 pores after impregnation, concentrated HNO_3 was added to lower the pH to <1. This is below the point of zero charge of SiO_2, which is around pH 4.[41]

Prior to each IWI, 2 g of silica gel (Davicat SI 1351; 340 m^2/g surface area, 1.20 ml/g pore volume, 15 nm pores) was dried for 1.5-2 hours at 200°C under vacuum. After cooling to room temperature under vacuum, the precursor solution was added dropwise to the powder under stirring. The amount of added precursor was 90% of the total pore volume, which yields a theoretical Co weight loading of 10%. Directly after impregnation, the flask was equilibrated (held under 'static' vacuum for 1 h) and then evacuated 24 h for drying. After drying the sample was stored inside a glovebox to ensure it would remain dry.

Heat treatments to decompose cobalt nitrate into cobalt oxides were performed with the following program: a temperature ramp of 2°C/min to 300°C, which was held for 60 minutes, under a flow of N_2 of 100 mL/g/min. Subsequent reduction of the cobalt oxides was performed at 450°C (ramp: 5°C/min) in a 10% H_2 in N_2 flow of 100 ml/g/min for 2 hours. The resulting Co/SiO_2 was stored in inert atmosphere, as contact with oxygen can rapidly oxidize Co. Three separate batches were made.

3.1.2 Deposition of Cu via Galvanic Replacement

All handling of chemicals prior to washing was performed under inert conditions, using both a glovebox and a Schlenk line. 200 mg of reduced Co/SiO_2 was loaded inside a flask, which then was attached to a water-cooled condenser. Solvents that were not stored inert (*i.e.* oxygen and water free) were dried prior to usage by heating under vacuum and degassed by de- and repressurizing with N_2 three times. The solvent was then added to a flask loaded with a copper salt to make the copper solution (typically 20 mL). The used copper solutions are shown in Table 2.

Table 2 – The used Cu precursors, solvents and reaction temperatures used for each galvanic replacement synthesis. The assigned name for each $CuCo/SiO_2$ catalyst is based on the precursor and solvent used.

Catalyst name	Cu precursor	Solvent	Reaction Temperature (°C)
CuCl/OLA	CuCl	Oleylamine	185
$Cu(acac)_2$/OLA	Cu(II)acetylacetonate	Oleylamine	185
CuCl/BTA	CuCl	*n*-butylamine	70
$Cu(acac)_2$/ACN	Cu(II)acetylacetonate	Acetonitrile	75
$Cu(NO_3)_2$/ACN	$Cu(II)(NO_3)_2$	Acetonitrile	75
$Cu(NO_3)_2/H_2O$	$Cu(II)(NO_3)_2$	Water	90

Next, 15 mL of copper precursor solution was added to the flask with Co/SiO_2 at room temperature, afterwards the mixture was heated and stirred for 20 hours. The temperatures used for each reaction are shown in Table 2. A schematic depiction of the setup is shown in SI figure 1. The particles were then washed by centrifugation and redispersion, first in the solvent used and then several times in ethanol. After washing the catalyst was dried at 120°C in static air. For CuCl/OLA, a slightly different

method of the above was used where both Co/SiO_2 and CuCl were loaded inside a flask together and then OLA was added. The concentration of the copper precursor solutions was in the order of 10 mM, the total amount of copper added was 40% of the total amount of Co atoms for Cu^+ precursors and 33% for Cu^{2+} precursors to get a theoretical ratio of 2:1 Co:Cu, with a 12% for Cu^+ and 10% total metal weight loading for Cu^{2+} precursors.

Heat treatments to remove potential remaining organic solvents after Cu deposition were performed on all catalysts. First, the catalysts were dried for 30 min at 120°C (temperature ramp: 5°C/min) in a N_2 flow of 200 mL/g/min and then another 30 min in synthetic air. Afterwards, the temperature was increased to 450°C (ramp: 5°C/min) and held for 1h in a synthetic air flow of 200 mL/g/min.

The CuCo catalysts prepared by galvanic replacement are named after the Cu precursor and solvent used during the galvanic replacement reaction.

3.1.3 Preparation of the co-impregnated reference catalyst

An impregnation solution was prepared with 1.3071g $Cu(NO_3)_2 \cdot 3\ H_2O$ (Acros Organics, Copper(II) nitrate trihydrate, 99%) and 3.3819g $Co(NO_3)_2 \cdot 6\ H_2O$ (Acros Organics, Cobalt(II) nitrate hexahydrate, 99+%) in a 10 mL volumetric flask with H_2O (Milli-Q), giving a Co concentration of 1.1620 M and Cu concentration of 0.54102 M. HNO_3 was added to lower the pH to <1. For this catalyst a hydrophilic fumed silica support (Aerosil® 300) was used (surface area 277 m^2/g, 0.783 ml/g pore volume). The same procedure was used as in 5.1.1 for the impregnation, which gives a theoretical loading of 5wt% Co and 2.5 wt% Cu. A ramp of 2°C/min to 300°C, which was held for 60 minutes, with a flow of N_2 of 200 mL/g/min) was used to calcine the catalyst.

3.2 Characterization

3.2.1 XRD

X-ray diffraction experiments were performed on either a Bruker D2 Phaser or a Bruker D8 Advance (for samples that need to stay in inert atmosphere). Co $K\alpha_{1,2}$ radiation (λ = 1.79026 Å) was used in all cases with a measured angle from 15 to 100° 2θ with an angle increment between each measurement of 0.12°. Crystallite sizes of measured samples were determined using the Scherrer equation.[42]

3.2.2 TEM

A Thermo Fischer Scientific (Formerly FEI) Tecnai T20 was used for BF-TEM analysis, operated at 200 kV.

A Thermo Fischer Scientific Talos F200X was used for STEM combined with high-angle annular dark-field (HAADF-STEM) and energy dispersive x-ray spectroscopy (EDX) analyses. This microscope was operated at 200 kV, and is equipped with a high-brightness field emission gun and a Super-X G2 EDX detector.

TEM samples were prepared by first suspending the particles in ethanol, followed by drop casting on a Ni (for EDX of Cu-containing samples) or a Cu grid. For particle size analysis, the number average was used.

3.2.3 TPR

Temperature programmed reduction was performed on Co/SiO_2 and $CuCo/SiO_2$ samples using a Micromeritics Autochem II chemisorption analyser equipped with a TCD. 50-80 mg of sample would be initially dried at 120°C for 30 minutes and cooled down back to room temperature. The measurement would then start in a 5% H_2/Ar mixture with a temperature ramp of 5°C/min to up to 900°C.

3.2.4 H_2-chemisorption

Hydrogen chemisorption was performed on Co/SiO_2 samples using a Micromeritics ASAP 2020 to determine the cobalt particle size prior to galvanic replacement. Samples were reduced at 450°C for 2 hours (heating ramp: 5°C/min) prior to the measurement. After reduction the samples were evacuated and cooled to 150°C, then measured at 150°C.

3.2.5 ICP-OES

All samples for ICP measurements were sent to and performed by Mikroanalytisches Laboratorium Kolbe, Germany according to in-house procedures.

3.3 Catalysis

3.3.1 Catalysis at varying temperatures

Catalytic testing was performed with an Avantium Flowrence 16 parallel reactor setup. 15 mg of catalyst (particle size: 75-150µm) diluted with 275 mg (particle size: 212-425µm) SiC was loaded in stainless steel reactors with an internal diameter of 2 mm. The catalysts were reduced *in-situ* at 450°C (temperature ramp: 5°C min^{-1}) in 10vol% H_2 in N_2 at 1 bar with a total flow of 175 ml min^{-1} divided over 16 reactors. The temperature was lowered to 120°C and the pressure was increased to 40 bar in synthesis gas with a H_2/CO ratio of 2/1 *V/V* (10 vol% He as internal standard). The temperature was then increased to 225°C, 250°C, 275°C and back down to 225°C (5°C min^{-1}) after 3 GC cycli per reactor (4.6h). The product stream was analyzed with an Agilent Technologies 7890B GC system using an FID for the hydrocarbon and alcohol products.

3.3.2 Isotherm catalysis run

The second catalytic run was performed in the same setup as 3.3.1. 10-65 mg of catalyst (particle size: 75-150µm, quantity was aimed to get 10% conversion based on the first run) diluted with 200-325 mg (particle size: 212-425µm) SiC was loaded in stainless steel reactors with an internal diameter of 2 mm. The catalysts were reduced *in-situ* at 450°C (temperature ramp: 5°C min^{-1}) in 10vol% H_2 in N_2 at 1 bar with a total flow of 175 ml min^{-1} divided over 16 reactors. The temperature was lowered to 120°C and the pressure was increased to 40 bar in synthesis gas with a H_2/CO ratio of 2/1 *V/V* (10 vol% He as internal standard). The temperature was then increased to 250°C (ramp: 5°C min^{-1}) for 80h, after which the pressure was increased to 60 bar. After 10 GC cycli at 60 bar, the gas flow was doubled.

4 Results

4.1 Preparing Co/SiO_2

Before (partial) galvanic replacement can be performed to obtain a bimetallic catalyst, a sacrificial template must be prepared. Co particles deposited on SiO_2 are used as the template, the results of the synthesis are reported in this section.

Three different batches were used for the catalysts, all prepared by the same methodology. The results are shown in Table 3. The final metal weight loading was slightly lower than the aimed for 10wt% for all three batches as determined by ICP. This is attributed to user error during impregnation, as the calculated amount added was 10 wt% for the three batches. The slightly lower weight loadings have no effect on the galvanic replacement itself, however a minor influence on the conversion during catalysis is expected due to the decrease of active metals. XRD was performed after the calcination of the impregnated samples, which shows that crystalline Co_3O_4 was formed and that the nitrate precursor was fully decomposed (SI figure 2). 450°C was used for the reduction temperature based on a TPR experiment performed (SI figure 6) to reduce the Co oxides to metallic Co, which is required for galvanic replacement. A diffractogram after reduction is shown in SI figure 2 as well, where both metallic Co and CoO peaks are visible. The presence of partially oxidized Co is due to the used equipment for inert diffraction experiments not being completely airtight.

Table 3 – Co weight loading and particle size (diameter) as determined by ICP for the former and TEM and H_2 chemisorption for the latter. The amount of particles counted by TEM is given in parentheses.

Batch	Co weight loading (%)	TEM particle size (nm)	H_2 chemisorption particle size (nm)
1	8.2	8.1 ± 2.3 (252)	12.0
2	9.7	6.1 ± 3.1 (50)	20.6
3	8.8	10.3 ± 3.2 (133)	18.3

The metallic Co/SiO_2 batches were further characterized by TEM, which are shown in Figure 6. Co is generally found in large clusters over the support, though non-clustered particles were found as well. Statistical analysis was challenging with EM techniques due to the poor contrast between metal and support particles at high magnification. This was especially the case for batch 2 (Figure 6b), so only few particles were counted. To complement the particle size analysis, H_2 chemisorption was performed as well (Table 3). The chemisorption measurements yielded an average particle size around twice as large as TEM, which is a reasonable agreement between techniques.

In conclusion, metallic Co on SiO_2 was successfully synthesized with particle sizes of around 10 nm.

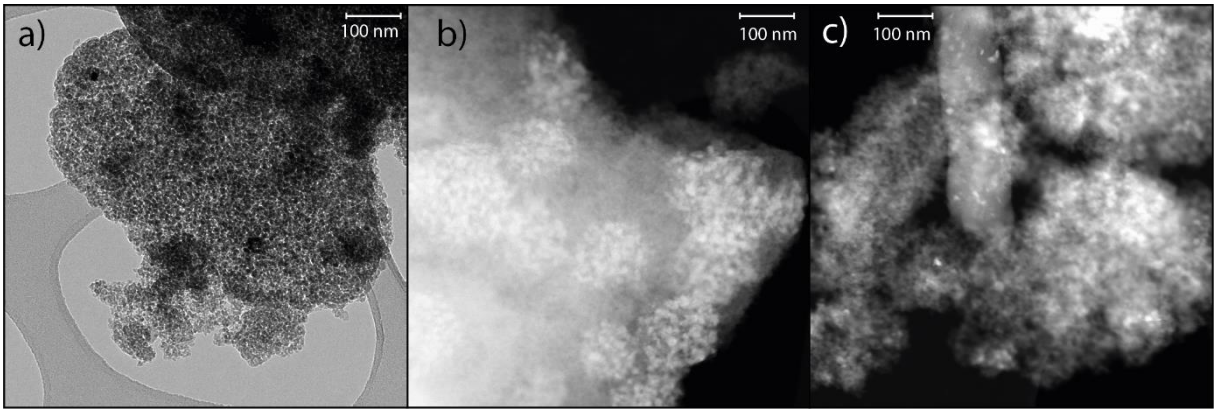

Figure 6 – BF-TEM (a) and HAADF-TEM (b and c) of batch 1, 2 and 3 respectively. Large metal clusters are more prevalent in batch 2 (b) than batch 1 (a) and 3 (c).

4.2 Deposition of Cu *via* Galvanic Replacement

4.2.1 ICP

In order to deposit Cu on Co/SiO_2 *via* the galvanic replacement reaction, the supported Co nanoparticles need to be immersed in a Cu solution. The choices for the solvents and precursors are first briefly discussed: oleylamine is used based on an adaptation of the work of Nafria *et al*.[19], where it was used in a mixture with o-dichlorobenzene as capping ligands for Co colloidal particles and to dissolve CuCl. *n*-butylamine was used as a shorter variant of oleylamine ($C_4H_{11}N$ compared to $C_{18}H_{37}N$) in an attempt to increase the degree of Co replacement by Cu. The reasoning behind this choice was that the GR reaction might have been limited due to poor diffusion into the pores of the SiO_2 support. Therefore, a shorter, more polar solvent might have better wetting of the support and diffuse into pores easier, facilitating more Cu deposition. Acetonitrile was selected based on the same idea, and water was used based on the work of Zhou *et al*.[26] CuCl was used as the initial Cu precursor, based on the work of Nafria *et al*. To investigate the possible effect of Cl poisoning on the $CuCo/SiO_2$ catalysts, Cl-containing and Cl-free Cu precursors were used. As other available Cu(I) salts have counterions that could poison the catalyst as well and are not easily removable either, Cu(II) precursors were opted for instead. Cu(II)acetylacetonate and $Cu(II)(NO_3)_2$ were used as both the nitrates and acetylacetonate (acac) groups could easily be removed by the heat treatment after galvanic replacement.

An overview of the successful galvanic replacement experiments is shown in Table 4. Comparing the theoretical Co and Cu weight loadings against the actual values after galvanic replacement in Table 4, it is clear that most precursor/solvent combinations performed the reaction considerably worse than 'perfect' galvanic replacement, that is 1) the 1:1 (or 1:2 for Cu^+) exchange ratio of Co for Cu^{2+} and 2) all copper from the solution reacting. This is shown visually in Figure 7. Instead, the Cu_{in}/Co_{out} ratio is in many cases lower than 1, which indicates that part of the Co is leached from the support without being replaced by Cu, which is undesirable. On the opposite side, there is an Cu_{in}/Co_{out} ratio of almost 3 for CuCl/OLA. Per the redox reaction equation, one metallic Co atom can only reduce two Cu^+ ions, so an excess of Cu_{in}/Co_{out} means that Cu is also incorporated into the catalyst in a different way. The most likely manner this excess Cu is added, is by it simply adsorbing onto the surface during the reaction and not being removed during the washing process. Cu incorporated into the catalyst this way is less likely to be in intimate contact with Co or present in a different form, both of which are undesirable as well.

Table 4 – Overview of all the different galvanic replacement experiments performed and the results. Initial Co wt% as determined by ICP. The columns 'theoretical wt%' are the values if 100% of the copper precursor added during the galvanic replacement reaction would have replaced Co.

Copper precursor	Solvent	Initial Co wt%	Co wt% after GR	Cu wt% after GR	Theoretical Co wt%	Theoretical Cu wt%	Co/ (Cu+Co)
CuCl	OLA	8.2	7.4	2.1	6.2	4.0	0.80
$Cu(acac)_2$	OLA	8.8	6.0	1.0	7.2	1.8	0.86
CuCl	BTA	9.7	6.0	1.7	7.6	4.0	0.80
[1]CuCl	BTA	9.7	6.4	2.0	-4.3	27.0	0.78
$Cu(acac)_2$	ACN	9.7	9.0	0.5	6.3	3.6	0.95
$Cu(NO_3)_2$	ACN	8.8	7.6	0.5	5.5	3.5	0.94
$Cu(NO_3)_2$	H_2O	8.8	6.0	3.3	5.5	3.6	0.66
[2]$Cu(NO_3)_2$	H_2O	8.8	5.8	3.5	5.5	3.6	0.64
[3]Co-impreg.	N/A	N/A	3.9	2.3	N/A	N/A	0.64

[1]Large excess of CuCl precursor was added. [2]Solvent was not degassed, Co/SiO_2 was briefly exposed to air prior to GR.
[3]Prepared by co-impregnation. N/A = not applicable, as this catalyst was not prepared via galvanic replacement.

Interestingly, in some cases the percentage of Cu deposition was roughly the same number depending on the solvent, even with different precursors. When using acetonitrile, only 13% of the Cu deposited on the catalyst from the solution in both cases, even though the initial Cu precursor concentration of $Cu(acac)_2$/ACN was half of $Cu(NO_3)_2$/ACN. For oleylamine, this was 51% and 57%, with Cu precursor concentrations equal. This is likely a coincidence and not an equilibrium as the same percentage was deposited in the first case despite different Cu^{2+} concentrations.

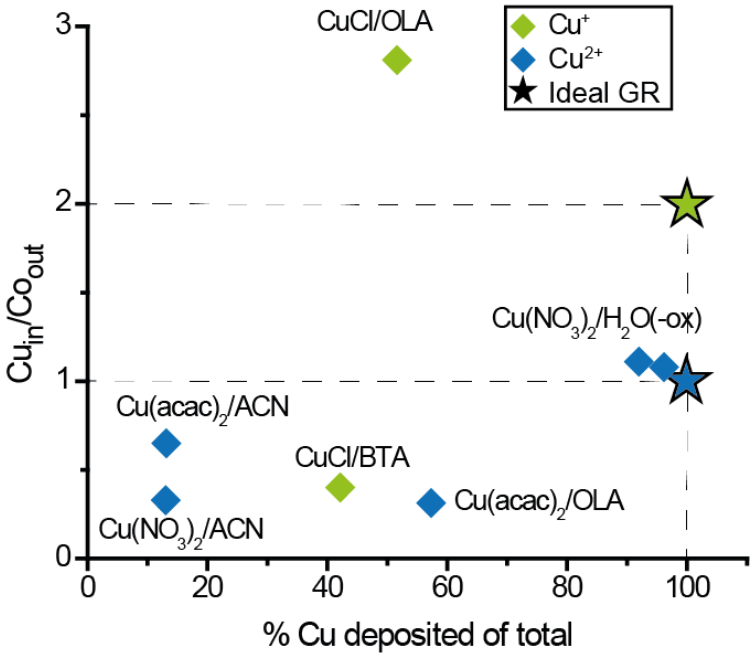

Figure 7 – The copper to cobalt exchange ratio from the galvanic replacement reactions plotted against the total deposited copper. A Cu_{in}/Co_{out} molar ratio of 1 and 2 for Cu^{2+} (blue) and Cu^{+} (green) respectively with a 100% Cu deposition is the ideal case, depicted with a star for each precursor.

Based on the results from Table 4 and Figure 7, changing from oleylamine to the shorter and more polar solvents acetonitrile and *n*-butylamine did not have a positive effect on the galvanic replacement. Instead it seems to have hindered the reaction instead, with the Cu deposition in acetonitrile dropping severely and *n*-butylamine leaching a lot of Co from the catalyst. Only water as a solvent yielded good results, as both the Cu deposition was high (92%) and the Cu_{in}/Co_{out} ratio is almost 1 (1.11).

Two different syntheses were repeated under slightly different conditions with the CuCl/BTA and $Cu(NO_3)_2/H_2O$ precursor/solvent combinations. For the former, a large excess of CuCl was used to test whether or not this would replace all the Co present on the support like it does for galvanic replacement of colloids (this catalyst is named +CuCl/BTA).[19] Despite over a fivefold increase of the Cu^{+} concentration, the weight loading of Cu only increased from 1.7 to 2.0 wt%. Due to the poor performance of CuCl/*n*-butylamine in the galvanic replacement reaction, solid conclusions cannot be drawn from this particular experiment. Instead, it should be repeated with an excess $Cu(NO_3)_2$ in H_2O as this Cu solution as this Cu solution performed the best in the galvanic replacement.

The redox reaction between Co and Cu requires metallic Co^0 and thus was performed in an oxygen-free environment during synthesis, but how detrimental would oxygen be for the galvanic replacement? To test this, the synthesis with $Cu(NO_3)_2/H_2O$ was repeated but first exposing the metallic Co to air for a minute and without degassing the solvent prior to GR (this catalyst is referred to as $Cu(NO_3)_2/H_2O$-ox). Against expectations, the galvanic replacement performed just as well with oxygen as with oxygen-free conditions, this is shown in Table 4 (denoted with [2]). It is clear that some oxygen is not detrimental to this reaction, though the extent of oxidation of Co prior to GR was not

determined. In order to test if the reaction is fully insensitive to oxygen, galvanic replacement should be attempted with fully passivated Co/SiO_2, *i.e.* a CoO shell with a metallic Co core to test whether CoO would form a 'barrier' and protect it from being replaced by Cu.

4.2.2 STEM-EDX

How much Cu was deposited was the first main question, the second one is where and how the Cu was placed relative to the Co. Several different techniques were used for this, but the most direct technique is TEM combined with EDX. This allows the direct observation of different elements, their distribution on the particle and the relative quantities of each element of a given area of interest. The TEM characterization of the as-synthesized $CuCo/SiO_2$ catalyst is shown.

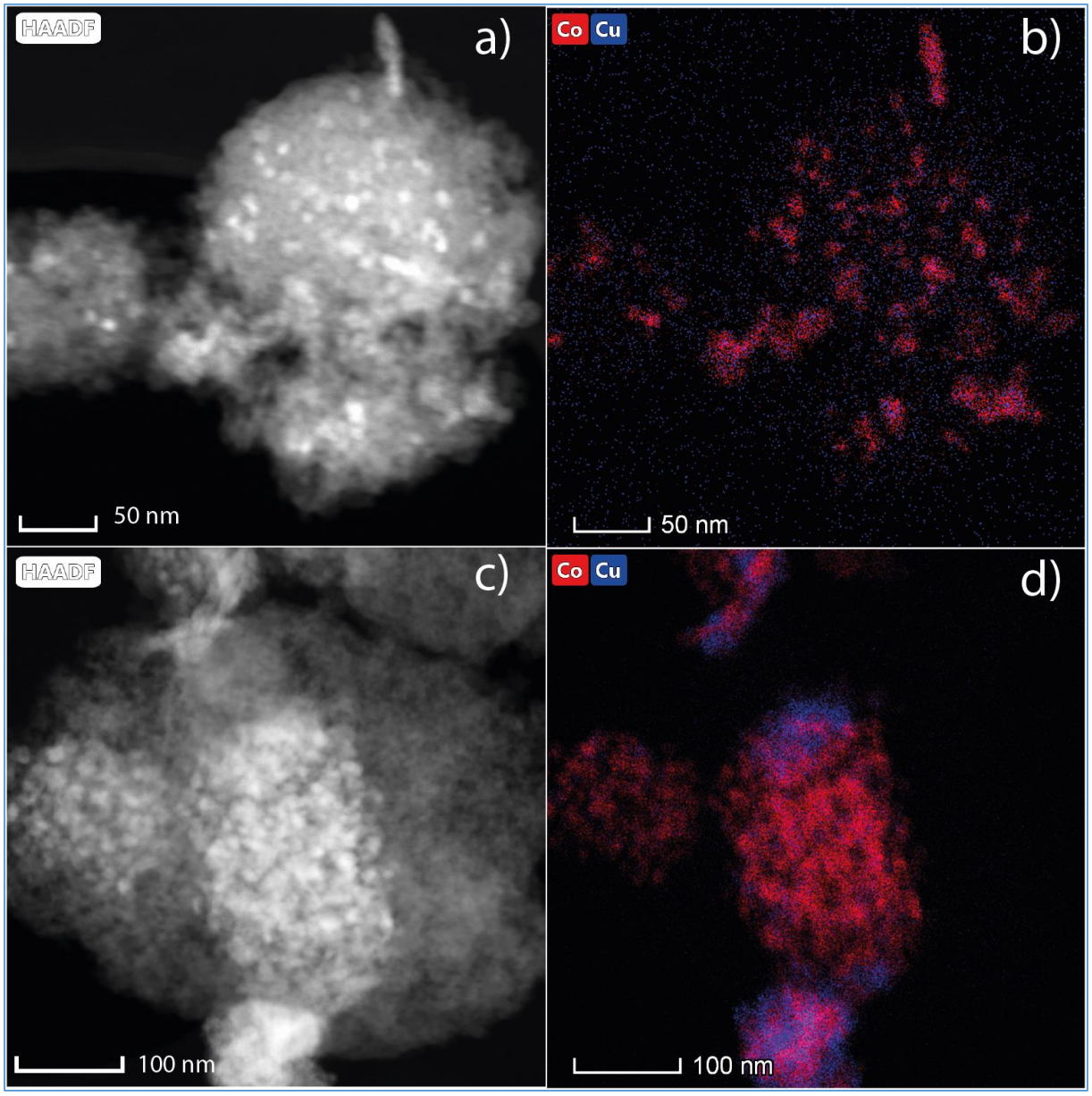

Figure 8 – STEM-EDX map of CuCl/OLA, showing the HAADF-STEM (a), STEM-EDX map of Co and Cu overlapped (b), and the HAADF-STEM (c) and EDX map (d) for a different particle of the same catalyst.

HAADF-STEM and EDX maps of CuCl/OLA are shown in Figure 8. The Co particles are clearly defined in the EDX map with little noise, especially compared to Cu. A Cu signal is still visible in the voids where there can be no support seen in the HAADF image. Despite the noise, there is still a higher Cu signal observable on top of the Co particles. This indicates that the selective deposition of Cu on top of Co was successful, though no conclusions can be drawn on the exact structure of the bimetallic particles formed due to the resolution and noise of the EDX maps. However, not all catalyst particles have this overlap of metals, an example is shown in Figure 8c and d. The metals were not homogeneously

distributed over the support on this particle, instead large clusters of smaller particles were formed. There are clear Cu hotspots on some parts of the Co clusters, while others are relatively Cu-deficient. Why some parts of the Co cluster were preferred over the other is hard to explain given the limited information obtained from a 2D STEM image. Possibly the Cu hotspots were on the surface of the support and thus Cu^+ ions were more likely to react with the Co here. Based on these images, galvanic replacement with oleylamine as a solvent and CuCl as copper precursor seems to lead to a good selective deposition of Cu on Co. However, the intimacy between metals is challenging to quantify based on a few EDX maps, and these images are not necessarily representative for all the catalyst particles. X-ray photoelectron spectroscopy (XPS) could help with determining the bimetallic structure, as it is a surface-sensitive technique that can be used to determine the surface molar metal ratios.[26]

The next catalyst discussed is CuCl/BTA. From the ICP results it was clear that this shorter organic solvent did not lead to a better Cu deposition (only 40%), and from Figure 9 it is also obvious that it did not lead to a selective deposition either. One large Co cluster (in red) is distinctly visible in both the EDX and HAADF images, unlike the Cu (in blue) which is dispersed all over the silica support without a real discernible increase of Cu on the Co cluster. This result suggests that the deposition of Cu was not via galvanic replacement, as a close intimacy between Cu and Co is expected based on the mechanism. It seems more likely that the Cu^+ precursor simply adsorbed onto the catalyst and was not washed off, though no peaks from the Cu^+ precursor were visible in XRD (Figure 14, page 23). Overall, *n*-butylamine is unsuitable for the galvanic replacement of supported nanoparticles.

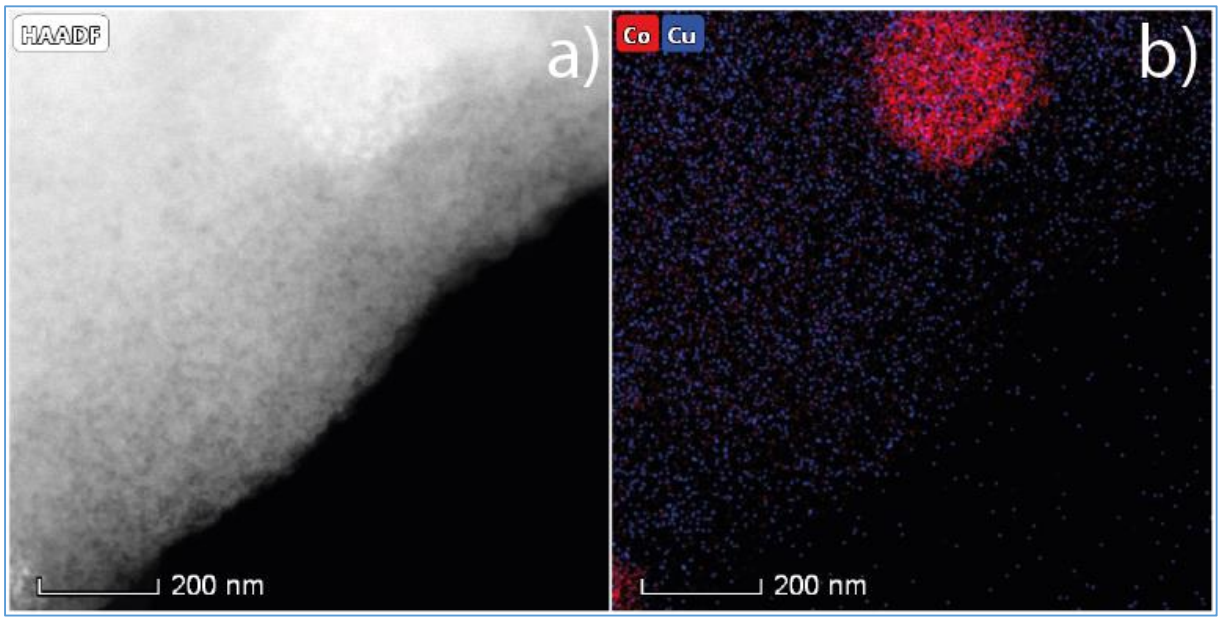

Figure 9 – STEM-EDX map of CuCl/BTA, showing the HAADF-STEM image (a) and the EDX map of Co and Cu (b). One large Co cluster is visible in red, whereas the Cu signal in blue is visible all over the silica support with an almost indiscernible increase of Cu on top of the Co cluster.

Similar results to CuCl/BTA can be seen in the TEM images of $Cu(acac)_2$/ACN, as shown in Figure 10. Distinct Co clusters (in red) are visible with dispersed Cu. However, the location Co clusters can be distinguished even in the Cu-only EDX maps (not shown), unlike in Figure 9. While this is a small improvement compared to CuCl/BTA, the selective deposition is still poor and the quantity deposited is as poor as well (13%), making acetonitrile an unsuitable solvent.

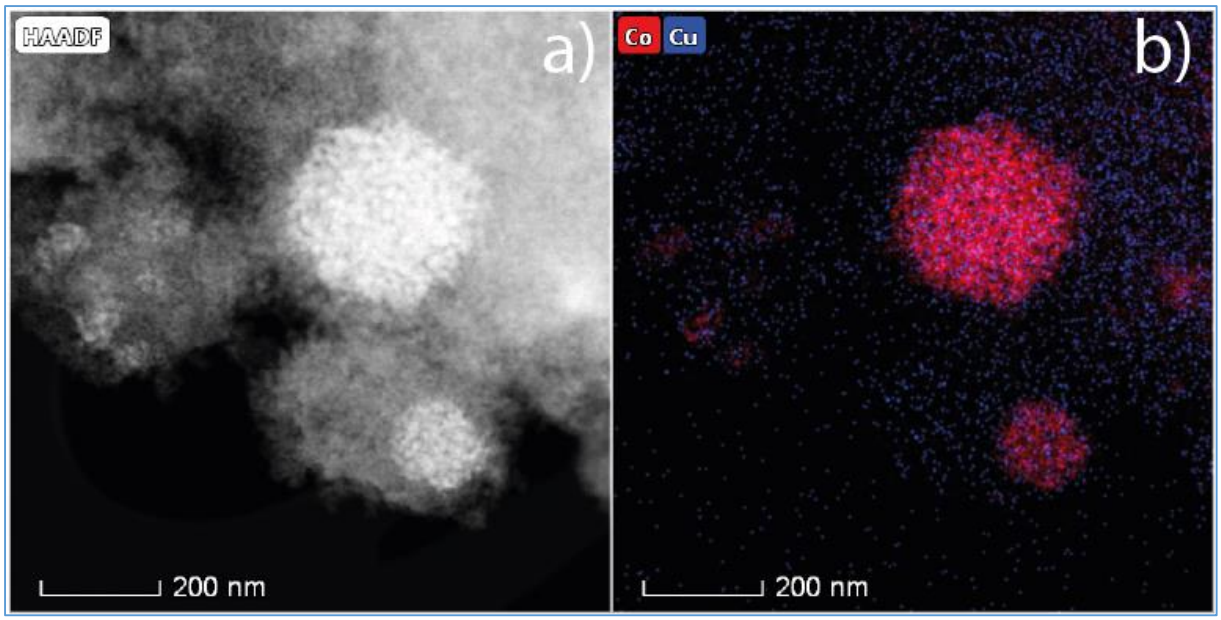

Figure 10 – STEM and EDX map of $Cu(acac)_2$/ACN, showing the HAADF-STEM image (a) and the EDX map of Co and Cu overlapped (b). Several large Co clusters are visible, with Cu dispersed all over the support.

The STEM-EDX images of the catalyst prepared with $Cu(II)(NO_3)_2/H_2O$ show something unexpected (Figure 11). Prior to galvanic replacement, distinct Co particles were visible in the EDX maps. After galvanic replacement, Co appears to have become more dispersed over the silica support. The Cu is mostly dispersed over the support as well, but a few Cu particles were spotted (see SI figure 3). This dispersion was not observed after the deposition in organic solvents. The increased dispersion could be due to the formation of cobalt silicates[43], however the exact mechanism is not known. The formation of cobalt silicates is discussed in more detail in section 4.3.3. Due to the Co dispersion, no hard conclusions could be drawn about the (un)selective deposition as it is not clear when this Co dispersion took place.

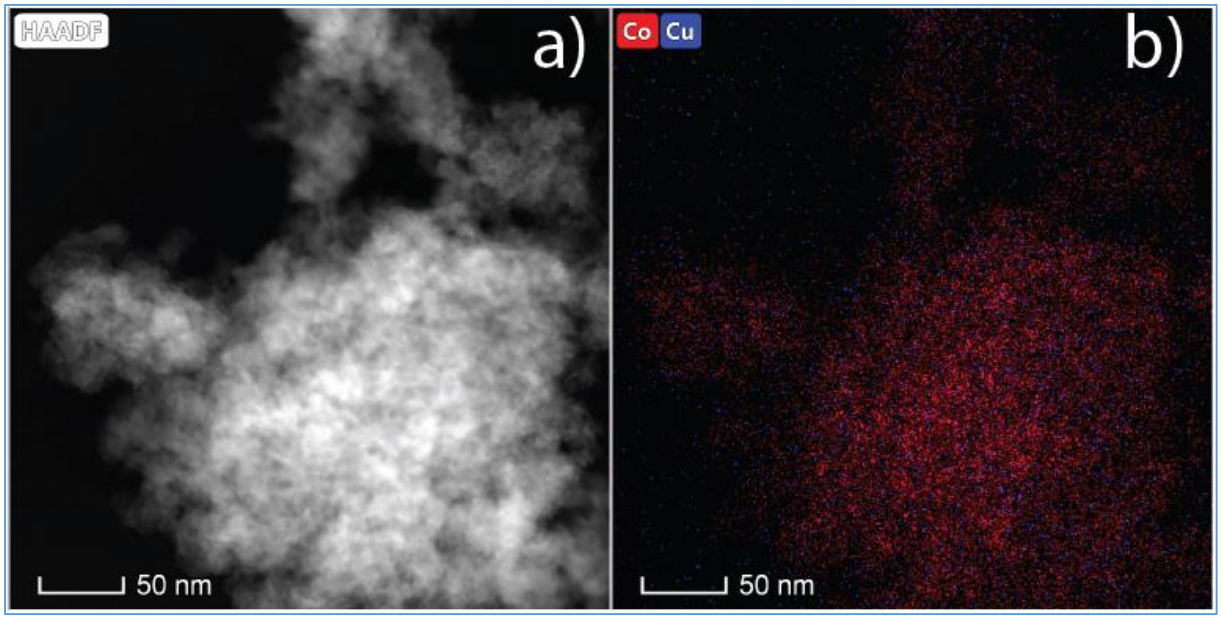

Figure 11 – STEM-EDX map of $Cu(NO_3)_2/H_2O$, showing the HAADF-STEM image (a), and the Cu (blue) and Co (red) EDX map overlapped (b). Both Cu and Co seem evenly dispersed over the support based on the EDX map.

Lastly, a CoCu catalyst has been prepared via co-impregnation as a reference to compare the metal intimacies between both methods. As shown in Figure 12, both metals seem very well mixed compared to the prior EDX maps of the GR catalysts. The metal particles are well dispersed over the support, with a constant Co to Cu ratio based on the EDX spectra (SI figure 4). By comparing Figure 12 with Figure 11, Figure 9 and Figure 8, co-impregnation appears to be the better choice for a good metal intimacy. However, $Cu(NO_3)_2/H_2O$ has the issue of the dispersed Co (silicate), so this catalyst cannot be directly compared to the co-impregnated reference. While EDX maps give a good indication of the metal intimacy, more advanced techniques such as XPS are required to draw definitive conclusions about which method leads to better intimacy.

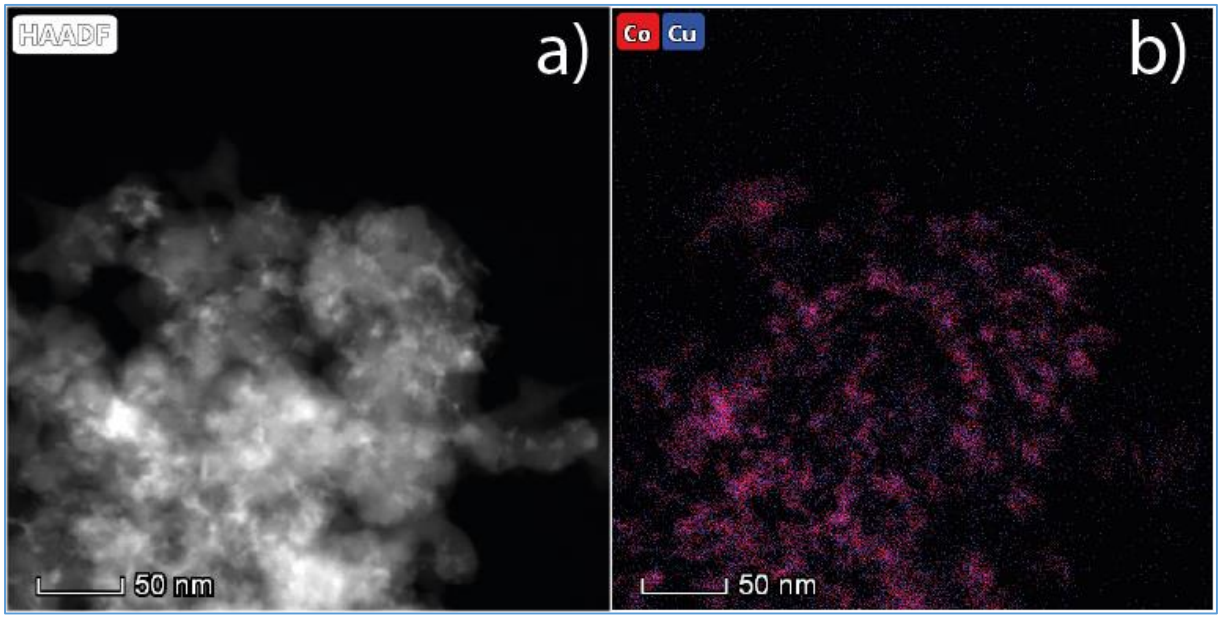

Figure 12 – STEM-EDX map of the co-impregnated reference catalyst, showing the HAADF-STEM image (a), and Co (red) and Cu (blue) overlapped (b). A very good overlap between metals can be seen on the Co and Cu EDX map (b).

4.2.3 TGA-MS

Some of the syntheses used rather long organic molecules such as oleylamine, which might still be present even after drying. In order to determine at which temperature these organics can be removed, TGA combined with MS was used with a synthetic air mixture (20% O_2/N_2) on catalyst CuCl/OLA. The plots are depicted in Figure 13. The TGA shows a minor loss in mass, though rather than a smooth line it jumps up and down. This is not the expected behaviour, as an increase indicates an increase in mass from an unknown source. The MS is according to expectations, showing peaks of CO_2, NO and H_2O simultaneously at slightly over 250°C. This corresponds to the burning of oleylamine from the catalyst, however another broad CO_2 peak is present at around 500°C without (detectable) accompanying H_2O or NO peaks. As only CO_2 was detected, some carbon might have formed on the catalyst after burning the oleylamine. Based on these results, the used oxidation temperature after galvanic replacement was 450°C.

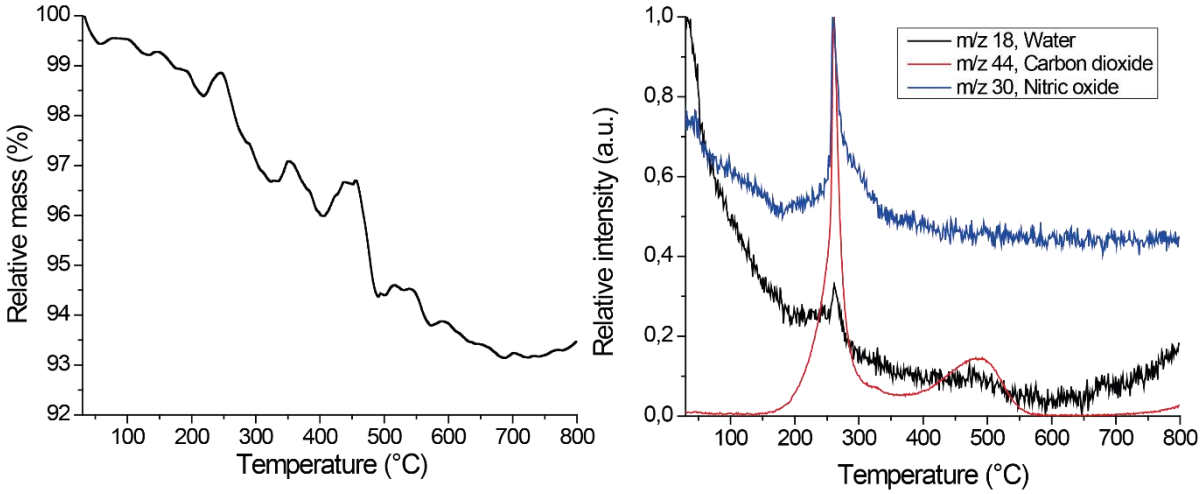

Figure 13 – TGA (left) and MS (right) measurements performed on CuCl/OLA. The black line corresponds to a m/z value of 18 (water), red m/z of 44 (carbon dioxide) and blue an m/z of 30 (nitric oxide). The removal of organics can be seen at 250°C, however an additional CO_2 peak at 500°C is also visible, of which the origin is unclear.

4.2.4 XRD

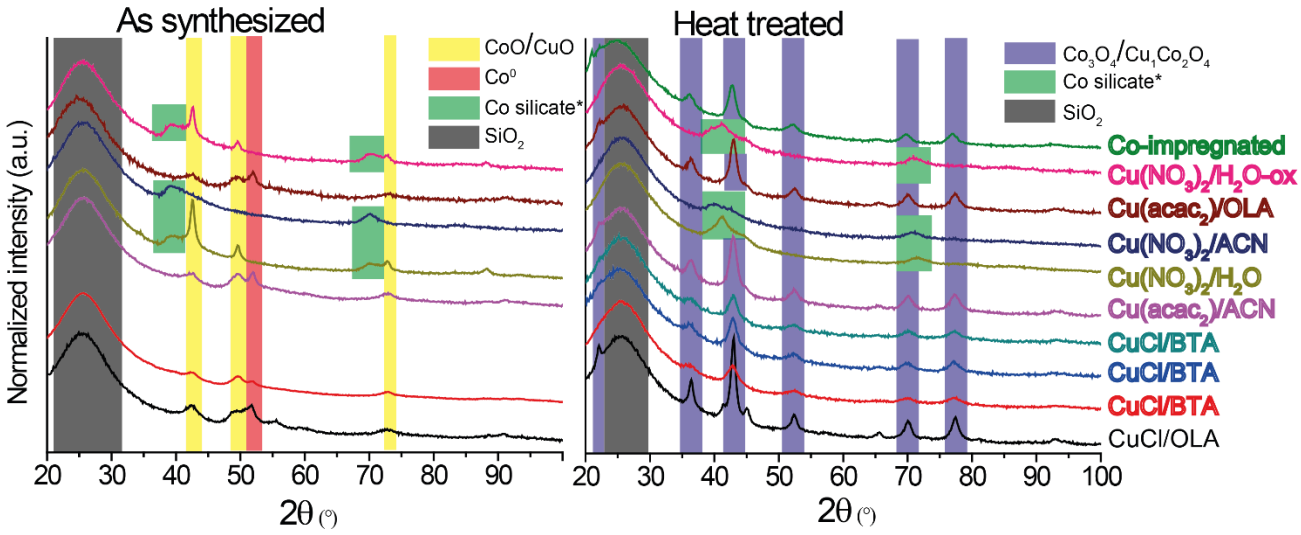

Figure 14 – X-ray diffractograms of $CuCo/SiO_2$ catalysts as synthesized via galvanic replacement (left) and after oxidation at 450℃ in 20% O_2 in N_2 (right). *Attributed to Co silicates based on TPR experiments. After oxidation, almost all diffractograms show the Co_3O_4 pattern, except for $Cu(NO_3)_2/H_2O$(-ox) and $Cu(NO_3)_2$/ACN.[44]

XRD experiments were performed to observe whether segregated bulk Cu was present and to obtain an indication of the crystallite size. In Figure 14 the XRD patterns of the as-synthesized (left) and heat treated (right) $CuCo/SiO_2$ catalysts are shown. The large, broad feature visible at 25° 2θ in all diffractograms corresponds to the amorphous silica gel support, indicated with a gray band. The peaks indicated with a yellow band of the as-synthesized catalysts correspond to either cubic CuO or CoO, which cannot be distinguished from each other due to the almost identical lattice parameters of these crystals. Catalysts $Cu(NO_3)_2/H_2O$(-ox) both show sharper peaks for the CoO/CuO crystallites (yellow), with the peak at 42° 2θ being the most prominent. This coincides with the superior galvanic replacement and the higher Cu weight loading (up to 3.5wt% compared to up to 2.3wt% of the rest) as shown by the ICP results (Table 4 and Figure 7). For $Cu(NO_3)_2$/ACN, neither CoO/CuO nor Co^0 (red band) peaks are visible, only two broad peaks at 40-45° and 70-73° 2θ (green bands) were present.

After oxidation (Figure 14, right) all CoO/CuO and Co^0 disappeared. Instead, $Co_3O_4/Cu_1Co_2O_4$ crystallites are visible (marked with blue bands) indicating that both Cu and Co were fully oxidized. As with CoO/CuO, Co_3O_4 and $Cu_1Co_2O_4$ have almost identical lattice parameters and thus cannot be distinguished.[44] Co_3O_4 is the main contributor to these peaks as the quantity of Cu in the catalysts is much lower than Co. However, no distinct CuO nor Cu_2O peaks are found in any of the oxidized catalysts despite the presence of up to 3.5wt% Cu. This indicates that the Cu in each catalyst consists of either (1) small, dispersed or otherwise non-crystalline particles or (2) incorporated into the mixed metal oxide. Option (1) is likely for the catalysts synthesized in butylamine and acetonitrile as the Cu was shown to be dispersed everywhere over the silica as seen in the STEM-EDX maps (Figure 9 and Figure 10) of the previous section. Option (2) is more likely for the co-impregnated and oleylamine synthesized catalysts, as the Cu was deposited on top of Co (Figure 12). For the three catalysts prepared with $Cu(NO_3)_2$ as Cu precursor, none of the Co_3O_4 peaks are visible after heat treatment despite the presence of 7.6wt% Co. Only the two broad peaks at 40-45° and 70-73° 2θ (green) are visible, which were also present prior to heat treatment. These catalysts were all exposed to water, during washing for $Cu(NO_3)_2$/ACN and as solvent for $Cu(NO_3)_2/H_2O$(-ox). The hypothesis is that the broad peaks are due to the formation of Co silicates, which is discussed further in section 4.3.3.

The crystallite sizes of the catalysts after oxidation were determined from the diffractograms using the Scherrer equation, which are shown in Table 5. The crystallite size is smaller than prior to GR as was shown in Table 3, this is likely due to the loss of Co being larger than the addition of Cu during GR for most catalysts as was discussed in section 4.2.1 (Figure 7). The exceptions are CuCl/OLA, which also shows the largest crystallite size, and both catalysts prepared with aqueous solutions which formed amorphous Co silicates.

Table 5 – Catalysts and their crystallite size after oxidation as determined with the Scherrer equation.

Catalyst	CuCl/OLA	CuCl/BTA	+CuCl/BTA	$Cu(acac)_2$ /ACN	$Cu(NO_3)_2$ /H_2O	$Cu(NO_3)_2$ /ACN	$Cu(acac)_2$ /OLA	$Cu(NO_3)_2$ /H_2O-ox
Crystallite size (nm)	12.0	6.8	6.8	7.5	4.6	4.4	8.4	4.5

4.2.5 TPR

In order to activate the CuCo catalysts, they need to be reduced. TPR was used on a heat treated CuCl/BTA catalyst to determine whether the reduction temperature has changed after introduction of Cu; the TPR profile is shown in Figure 15. No distinct Cu peak was visible in the TPR profile which is expected at 210°C[45], despite the 0.74 wt% Cu present. Because the addition of Cu makes Co oxides more easily reducible[45], 450°C was used for the *in-situ* reduction as this is a higher temperature than the CoO → Co peak even with a low Cu loading. A part of the metals will not be reduced at this temperature however, as a cobalt silicate peak at 650°C is still present.[43] Comparing this TPR profile to SI figure 6, the Co_3O_4 → CoO peak has shifted to a higher temperature by around 50°C while the CoO → Co peak has shifted to a lower temperature by around 50°C. This is in partial agreement with aforementioned literature, which claimed that the Co_3O_4 should shift to lower temperatures as well upon addition of Cu.[45]

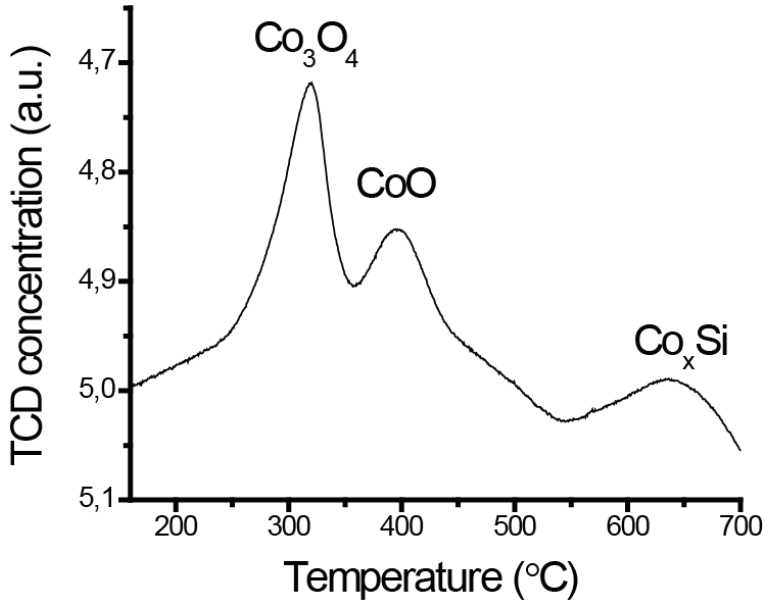

Figure 15 – TPR profile of CuCl/BTA. This profile was presumed to be representative for the reduction of all CuCo catalysts synthesized. Three peaks are visible, from left to right: The reduction of Co_3O_4, CoO and cobalt silicates respectively.[43,46] No distinct Cu reduction peak is visible.

4.3 Catalysis

Two CO hydrogenation tests with nine of the synthesized catalysts have been performed, which are shown in Table 6. The first test was performed at different temperatures (225 °C, 250 °C and 275 °C) to observe the effects on product selectivity and catalyst activity. The second test was performed isothermally at 250 °C to test the stability over a longer period.

Table 6 – $CuCo/SiO_2$ catalysts tested in the CO hydrogenation reaction with the metal weight loading and molar Co fraction of each catalyst.

Symbol	*Catalyst*	*wt% Co*	*wt% Cu*	*Co/(Cu+Co)*
■	CuCl/OLA	7.39	2.05	0.80
●	CuCl/BTA	6.01	1.67	0.80
▲	+CuCl/BTA	6.44	1.97	0.78
▼	$Cu(acac)_2$/ACN	9.01	0.47	0.95
◀	$Cu(NO_3)_2/H_2O$	6.01	3.33	0.66
▶	$Cu(NO_3)_2$/ACN	7.60	0.46	0.95
◆	$Cu(acac)_2$/OLA	5.99	1.02	0.86
⬟	$Cu(NO_3)_2/H_2O$-ox	5.80	3.48	0.64
⬢	Co-impregnated	3.87	2.34	0.64

4.3.1 Catalytic activity at 225°C, 250°C and 275°C.

The performance of the $CuCo/SiO_2$ catalysts in CO hydrogenation is shown in Figure 16. The graph is divided into 4 regions which each correspond to a different reactor temperature (225°C, 250°C, 275°C and 225°C again respectively) with a plot focussing on the region of 0-5% CO conversion below. There is an obvious increase in CO conversion when the reactor temperature is increased for most catalysts, ranging from 8 to 16 times increase in conversion when the reactor temperature goes from 225 to 275°C. For ◀ $Cu(NO_3)_2/H_2O$, ▶ $Cu(NO_3)_2$/ACN and ⬟ $Cu(NO_3)_2/H_2O$-ox no activity was observed due to not being reduced due to Co silicate formation, which is discussed in section 4.3.3. Despite the similar weight loadings, large differences in CO conversion are observed. The highest conversion is achieved by ◆ $Cu(acac)_2$/OLA with 5.99/1.02wt% Co/Cu while the second highest is ▼ $Cu(acac)_2$/ACN with 9.01/0.47wt% Co/Cu, despite Cu decreasing the activity of the catalyst.[21,47] The difference could be due to different particle size distributions, however they were nearly the same size prior to reduction with a crystallite size of 7.5 and 8.4 nm respectively (Table 5, page 24). All catalysts gradually deactivate, which is most prominently visible in the 275°C region.

Table 7 shows the products of the CO hydrogenation at the second data point of each temperature. The products are primarily straight chain alkanes in the C_1-C_7 range, with hydrocarbon (HC) selectivities ranging from 92 to 98%. The high HC selectivity indicates that the CO is infrequently incorporated into the growing carbon chains, which could be due to segregation of both metals. Segregated Co domains act as FTS catalysts, which results in HC formation. The primary HC formed is methane with a selectivity ranging from 40 to 70%, depending on the catalyst. The higher alcohol selectivity (C_{2+} ROH) is low, with 0-2% at 225°C but with a clearly higher selectivity by increasing the temperature to 250°C and 275°C, where the products are around 4% HA. Methanol production is only produced at higher temperatures as well, with no methanol detected for any catalyst at 225°C. Interestingly, the co-impregnated catalyst has a relatively much higher methanol selectivity compared to the GR CuCo catalysts; 0.84% to 0.22% at 250°C and 2.26% to 0.73% at 275°C for the co-impregnated and the second 'best' methanol producing catalyst, $Cu(acac)_2$/OLA. This could be due to the higher Cu/Co ratio for the co-impregnated catalyst, or due to differences in synthesis method (*i.e.* co-impregnation and galvanic replacement) leading to different catalyst structures (*e.g.* surface composition). The former hypothesis can be tested

by varying the Cu:Co ratio, while the latter requires advanced characterization techniques like XPS. The higher alcohol products consist primarily of C_2 and C_3 alcohols, with only $Cu(acac)_2$/ACN and $Cu(acac)_2$/OLA yielding detectable amounts C_{6+} alcohols (1.3% and 0.9% at 275°C respectively) at 250°C and 275°C.

Based on these results the second CO hydrogenation test was performed at 250°C, as 225°C yielded very little alcohols and while catalysis at 275°C yielded the most desired products, it also deactivated more rapidly.

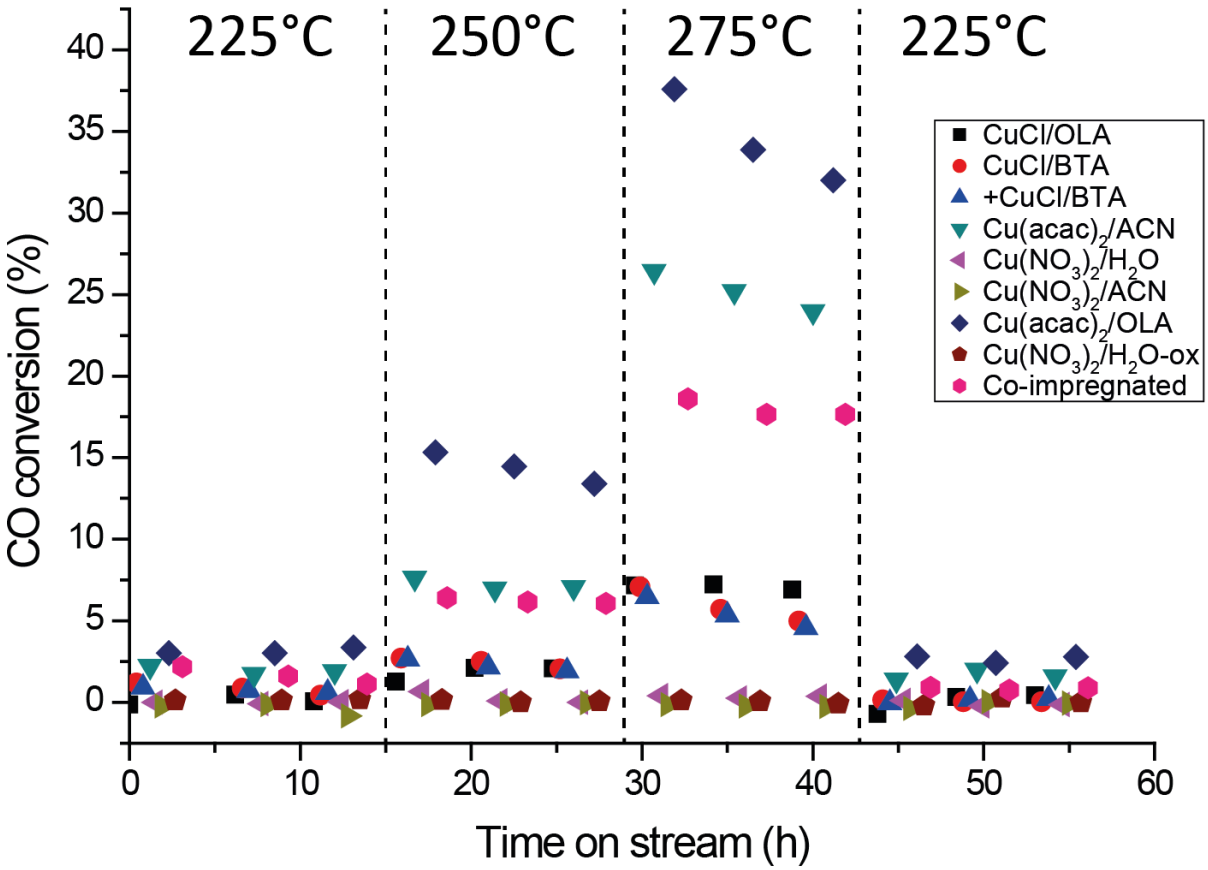

Figure 16 – The conversion of the $CuCo/SiO_2$ catalysts plotted against the time on stream – H_2/CO = 2/1 V/V, P = 40 bar, GHSV = 3300 h^{-1}, T = 225°C, 250°C, 275°C, 225°C for each region bordered by a dashed line respectively. The same figure plotted from 0 to 5% conversion is shown below.

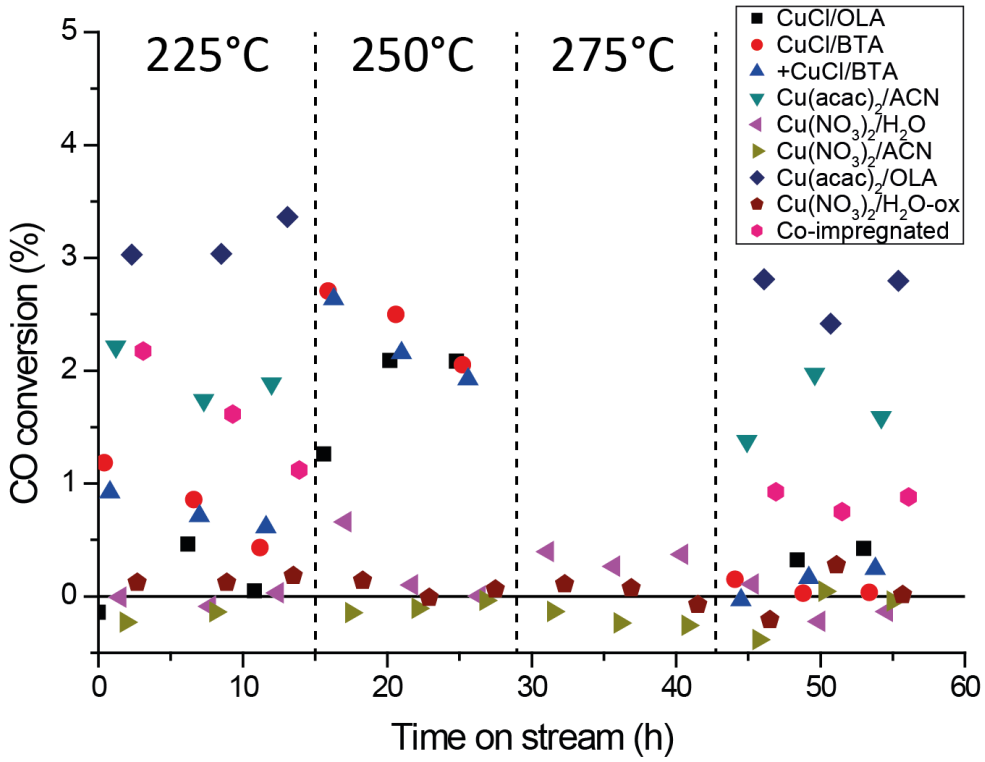

Table 7 – Product selectivities, metal time yield and CO conversion based on the third measurement point at 225, 250 and 275°C for each active $CuCo/SiO_2$ catalyst.

Catalyst	T (°C)	MTY ($\frac{\mu mol\ CO}{g_{CuCo} * s^{-1}}$)	CO conversion (%)	Selectivity C_{2+} ROH (%)	Selectivity other oxy (%)	Selectivity total oxy (%)	Selectivity HC total (%)	Selectivity methanol (%)	Selectivity methane (%)	Selectivity ethanol (%)	C Mass balance (%)
CuCl/OLA ■	225	0.17	0.05	0	0	0	97.82	0	59.68	0	100.35
	250	7.55	2.09	3.09	0	3.09	94.87	0	53.81	1.5	100.3
	275	26.02	7.22	4.36	0	4.88	93.09	0.51	51.29	1.72	100.24
CuCl/BTA ●	225	3.45	0.86	2.76	0	2.76	95.81	0	50.91	2.76	100.32
	250	10.10	2.5	4.17	0	4.17	94.27	0	54.07	2.47	100.27
	275	23.46	5.69	4.81	0	5.11	93.38	0.3	53.54	2.76	100.26
+CuCl/BTA ▶	225	3.14	0.71	2.99	3.14	6.13	92.43	0	53.43	2.99	100.33
	250	9.41	2.16	3.65	0	3.65	94.71	0	54.73	2.23	100.29
	275	24.05	5.36	4.37	0	4.37	94.09	0	54.65	2.5	100.25
$Cu(acac)_2/ACN$ ◀	225	6.30	1.74	0.52	1.64	2.17	96.56	0	41.82	0.52	100.3
	250	24.54	6.96	3.45	0.63	4.08	94.54	0	41.46	0.97	100.19
	275	88.90	25.18	4.71	0.3	5.57	92.25	0.56	41.68	1.15	99.83
$Cu(acac)_2/OLA$ ◆	225	14.88	3.03	1.26	0.89	2.16	96.91	0	39.76	0.39	100.29
	250	71.02	14.45	4.06	0.41	4.69	94.35	0.22	36.17	0.73	99.96
	275	165.7	33.87	4.67	0.34	5.75	92.07	0.73	38.81	0.91	99.63
Co-impregnated ●	225	9.18	1.62	2.66	0	2.66	96.86	0	49.59	1.2	100.32
	250	34.06	6.16	4.05	0.18	5.07	94.44	0.84	50.05	1.71	100.23
	275	99.67	17.65	4.31	0.14	6.71	92.64	2.26	51.55	1.69	100.11

4.3.2 160h isotherm CO hydrogenation

For the second catalytic test, different amounts of catalyst were loaded to run at a similar conversion. Because of this, the metal time yield (MTY) is used to compare activity. The MTY against the time on stream of the active $CuCo/SiO_2$ catalysts in CO hydrogenation is plotted below in Figure 17. Initially all catalysts deactivate rapidly, after which the deactivation slows down. The exception is the co-impregnated catalyst, which shows a consistent rate of deactivation rather than a large initial drop. The rate of deactivation is given in Table 8, where the MTY of 10h and 70h on stream is compared. $Cu(acac)_2$/OLA is still the most active followed by the co-impregnated catalyst. CuCl/OLA and $Cu(acac)_2$/ACN are the most stable catalysts from the 10-70h period, with 70% of the activity compared to 10h on stream remaining. Catalysts CuCl/BTA and +CuCl/BTA lose the most activity, dropping almost 50% in the first 10h on stream, and losing 50-65% more in the following 60h. A possible explanation is that the large Co clusters of smaller particles (section 4.2.2, Figure 9) coalesced into several larger particles leading to a drop in metal surface and thus activity. However, $Cu(acac)_2$/ACN did not show the same drop in activity despite having large Co clusters initially as well, so it is unclear where these differences in deactivation originate from.

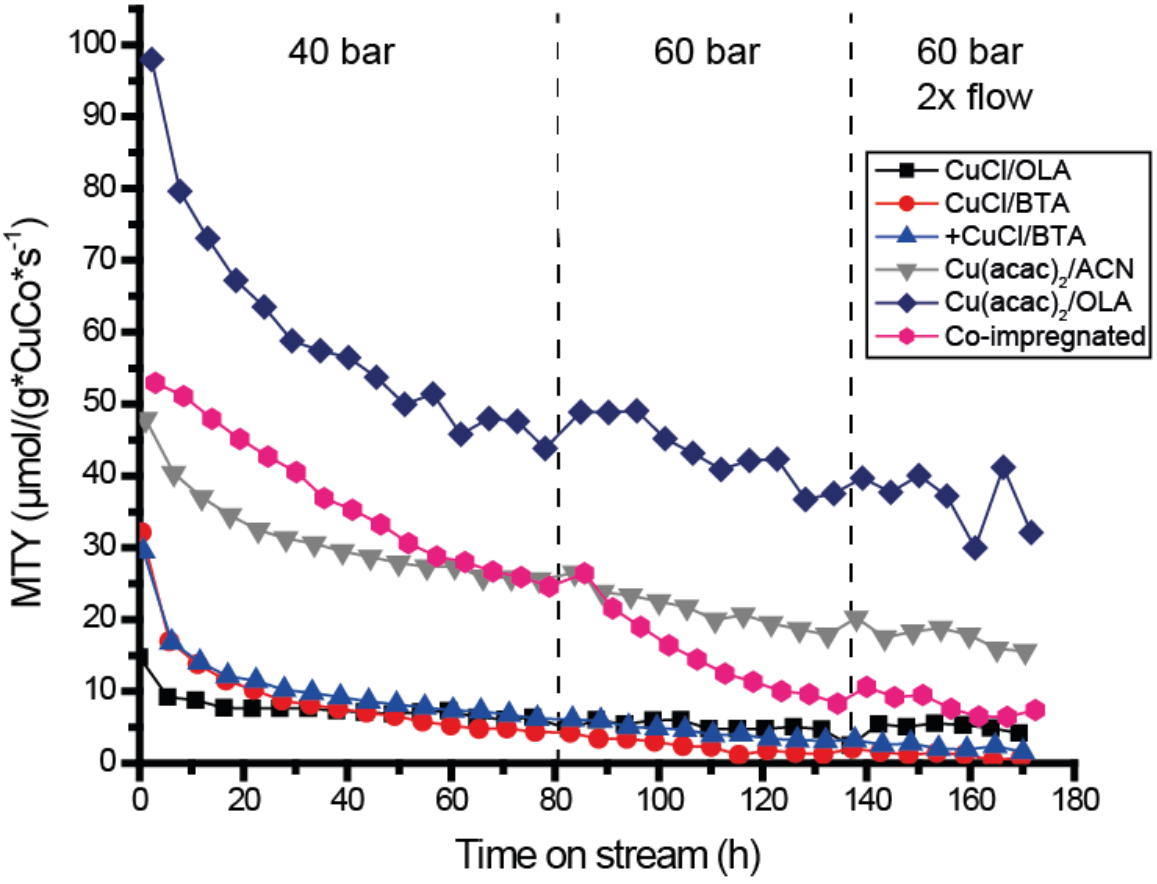

Figure 17 – The metal time yield (MTY, µmol CO converted/(g*CuCo*s^{-1})) of the $CuCo/SiO_2$ catalysts plotted against the time on stream – H_2/CO = 2/1 V/V, P = 40 bar (left region); 60 bar (center and right), GHSV = 820-5000 ml h^{-1}, T = 250°C. The gas flow is doubled in the third region. Activity with respect to initial is calculated by dividing the 14th measurement point (70-75h) by the 3rd (11-16h)

Table 8 – $CuCo/SiO_2$ catalysts tested in the second CO hydrogenation reaction with the metal weight loading, molar Co fraction and GHSV of each. Deactivation is calculated by dividing the 14th measurement point (70-75h) by the 3rd (11-16h).

Symbol	*Catalyst*	*wt% Co*	*wt% Cu*	*Co/(Cu+Co)*	*GHSV (h^{-1})*	*Activity after 70h on stream (%)*
	CuCl/OLA	7.39	2.05	0.80	1480	69.6
	CuCl/BTA	6.01	1.67	0.80	1100	35.0
	+CuCl/BTA	6.44	1.97	0.78	820	48.2
	$Cu(acac)_2$/ACN	9.01	0.47	0.95	2450	69.8
	$Cu(acac)_2$/OLA	5.99	1.02	0.86	5000	65.1
	Co-impregnated	3.87	2.34	0.64	2100	54.0

The reaction products from each catalyst are shown in Figure 18 after 70h on stream. As before, the desired higher alcohol selectivity is low (ranging from 1.8 to 6%). Of the higher alcohols produced, ethanol and propanols are the main products (Figure 19). For $Cu(acac)_2$/ACN, CuCl/OLA and the co-impregnated catalyst, the fraction of propanol is larger than ethanol. The only catalyst consistently producing a measurable amount of methanol is the co-impregnated catalyst as depicted in blue in Figure 18 (left). No clear trend is observed for higher alcohol selectivity regarding the Co/(Cu+Co) ratio, which is shown in Figure 18(right). While the alcohol selectivity appears to slightly increase when a higher fraction of Cu is present, with the exception of $Cu(acac)_2$/OLA. Interestingly, the catalysts prepared by galvanic replacement have a similar to slightly better higher alcohol selectivity than the co-impregnated catalyst, despite the latter being closer to the optimal Co/(Cu+Co) ratio.[20] Moreover, the co-impregnated catalyst also appeared to have a better metal intimacy in the EDX maps (section 4.2.2), which also should result in a better HA selectivity based on the dual site mechanism.[20–22] These results contradicting with theory could point towards an advantage of synthesis *via* galvanic replacement, though other variables such as the different metal precursors could have caused this difference as well.[17] The catalysts synthesized via galvanic replacement with $Cu(NO_3)_2/H_2O$, which had the same precursors and Co/(Cu+Co) ratios as the co-impregnated catalyst, would have been the ideal comparison. However, these were inactive due to Co silicate formation during drying. When this silicate formation can be avoided, an active $Cu(NO_3)_2/H_2O$ catalyst should be compared to the co-impregnated catalyst to obtain the most convincing results about the (dis)advantageous effects of synthesis via galvanic replacement.

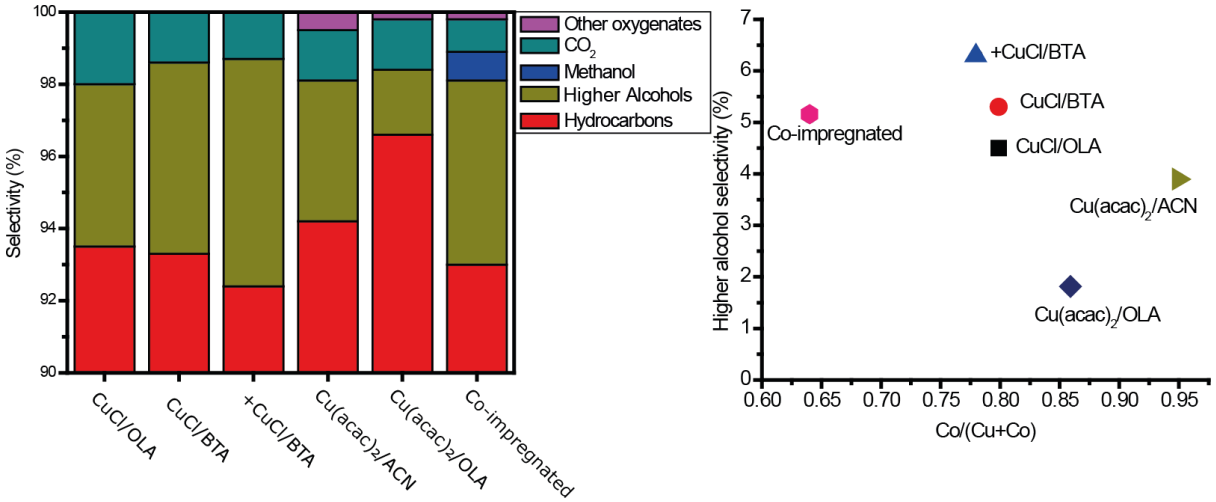

Figure 18 – (Left) Product distributions of each catalyst at T=250°C, 70-75h on stream, H_2/CO = 2/1 V/V and P = 40 bar. 0-90% is hydrocarbons only, primarily methane (around 50%). (Right) The higher alcohol selectivity plotted against Co/(Cu+Co) ratios of each catalyst.

In Figure 19 the hydrocarbon and alcohol product distribution by chain length for each catalyst is shown at 70-75h on stream. $Cu(acac)_2$/ACN produces the highest alcohol up to octanol and with hydrocarbons up to C_{15} (not shown). Long-chain higher alcohol production appears to be paired with long-chain hydrocarbon production, which is not unexpected considering the shared chain growth mechanism as described in section 2.1. The reverse is not true, however. This can be seen for $Cu(acac)_2$/OLA, where only up to propanol is produced despite the production of C_{10+} hydrocarbons. An explanation for this is that the Cu and Co are not intimate in this particular catalyst, which is supported by the fact that it is considerably more active (Figure 17) and has a low higher alcohol selectivity (Figure 18), which both point towards segregated Co.[47]

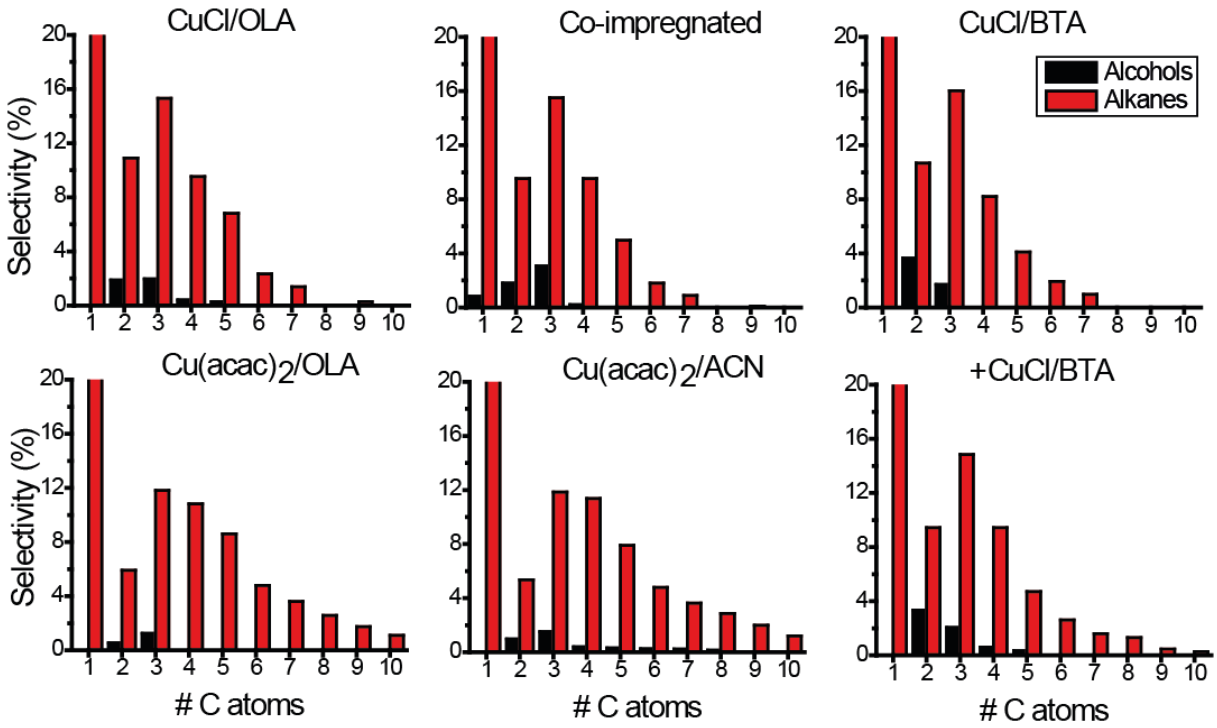

Figure 19 – Product distribution of each $CuCo/SiO_2$ catalyst (T= 250°C, 70-75h on stream, P = 40 bar, GHSV= 820-5000 h^{-1}, H_2/CO = 2/1 V/V) Red bars are alkanes, black bars are alcohols. The y-axis is cut-off at 20%, CH_4 exceeds >30% in all cases.

Another interesting observation is that longer-chain higher alcohol formation is more favoured at the start of catalysis, after which the alcohol production shifts to shorter alcohols such as C_2 and C_3. This can be seen in Figure 21, which shows the alcohol selectivities over time of +CuCl/BTA. In this figure a downwards trend of C_4-C_8 alcohols is visible, after 20h on stream no more heptanol nor octanol is detected. This decrease in long-chain products is also visible for the alkanes, this correlation is likely due to the linked mechanism for HAS and FTS as explained in section 2.1. This downward alcohol and alkane trend over time is less pronounced for the more stable catalyst $Cu(acac)_2$/ACN, which can be seen in Figure 20. This indicates that the decrease in chain growth probability is linked to the deactivation of the catalysts.

The decrease in chain growth probability over time is completely in line with the work of Yang *et al.*[6] They determined that the deactivation and decrease in chain growth probability of CuCo catalysts is due to "severe sintering" and "Co_xC formation on the catalyst surface" which both decrease the amount of surface Co atoms. The sintering of metal particles was also observed during the spent catalyst analysis, of which EDX images can be seen in SI figure 8.

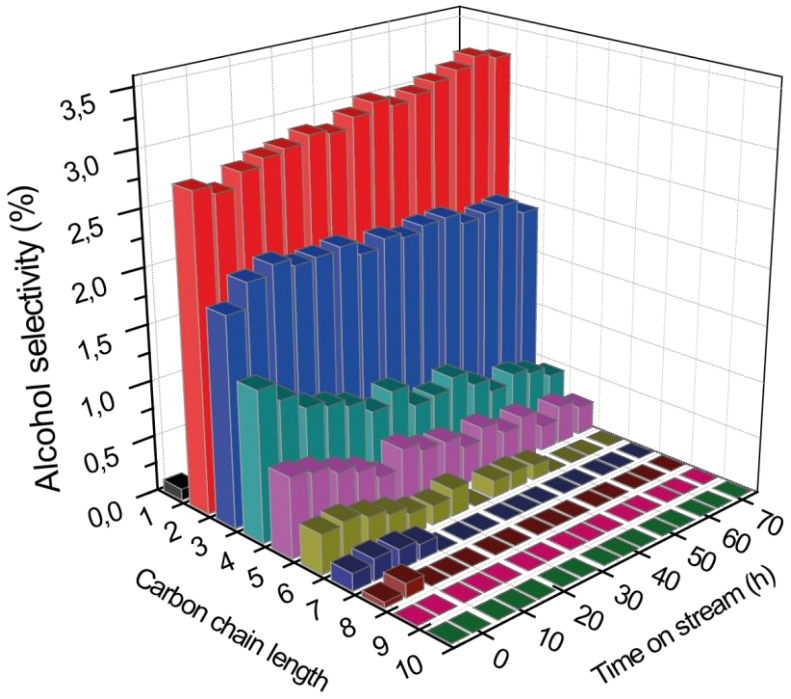

Figure 21 – Alcohol selectivities over time of +CuCl/BTA during the isothermal CO hydrogenation. The alcohol selectivity is of the total product selectivity. A declining trend for C_4-C_8 alcohols is visible over time. T=250°C, H_2/CO = 2/1 V/V, P = 40 bar and GHSV = 1100 h^{-1}.

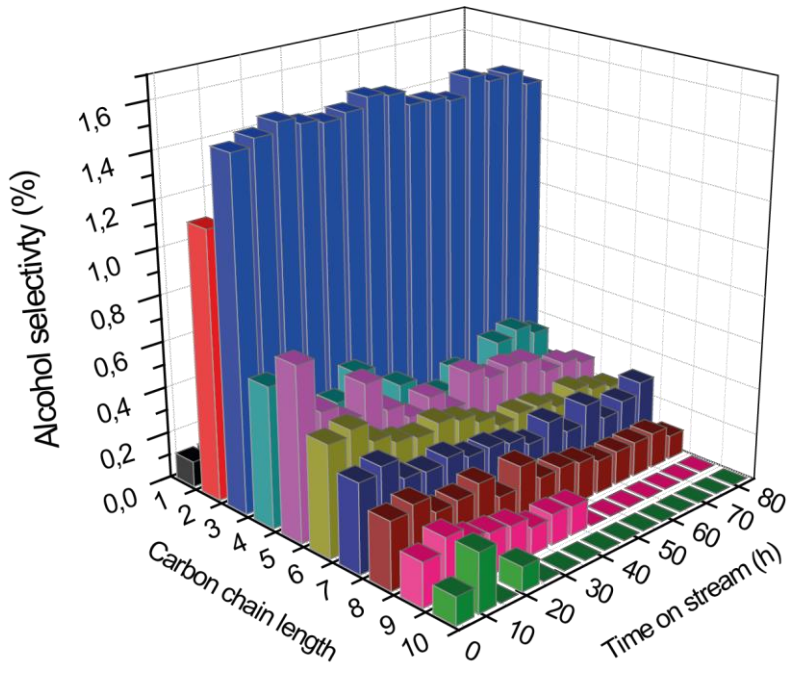

Figure 20 – Alcohol selectivities over time of $Cu(acac)_2$/ACN during the isothermal CO hydrogenation. The alcohol selectivity is of the total product selectivity. The alcohol selectivity does shift to shorter alcohols over time, but less pronounced. T=250°C, H_2/CO = 2/1 V/V, P = 40 bar and GHSV = 2450 h^{-1}.

4.3.3 Inactive catalysts

One of the first observations of the catalytic testing was that several catalysts were completely inactive. All of the inactive catalysts were a light brown-yellowish color unlike the active catalysts, which all were dark brown to black (Figure 22). There are several possible explanations as to why these catalysts can be inactive:

1) The reactant gas flow is too high for any (significant) conversion
2) Very few active sites due to a large amount of sintering
3) Active metals are not properly reduced

If the first possibility was the case, it would be expected that all catalysts show very little to no conversion. However, if we look at Figure 17, we can see that doubling the flow does not lower the MTY, it actually increases slightly. The decrease in conversion is due to the increased gas feed flow without a significant change in activity. As the MTY of the inactive catalysts was consistently <1 µmol/g CuCo/s, it seems unlikely that the inactivity is due to the reaction conditions.

If all metal particles sintered to a significant degree, the amount of available active sites would be severely limited which would cause a low MTY and thus conversion. It is possible that the metals sintered during either the heat treatment or reduction prior to catalysis, or rapid sintering when exposed to the syngas. However, if we look at the diffractogram of the inactive catalysts (Figure 23) and apply the Scherrer equation to get an indication of the crystallite size, very large crystallites do not appear to be present after heat treatment. Only two broad peaks are visible in the 40-45° and 70-73° 2θ range.

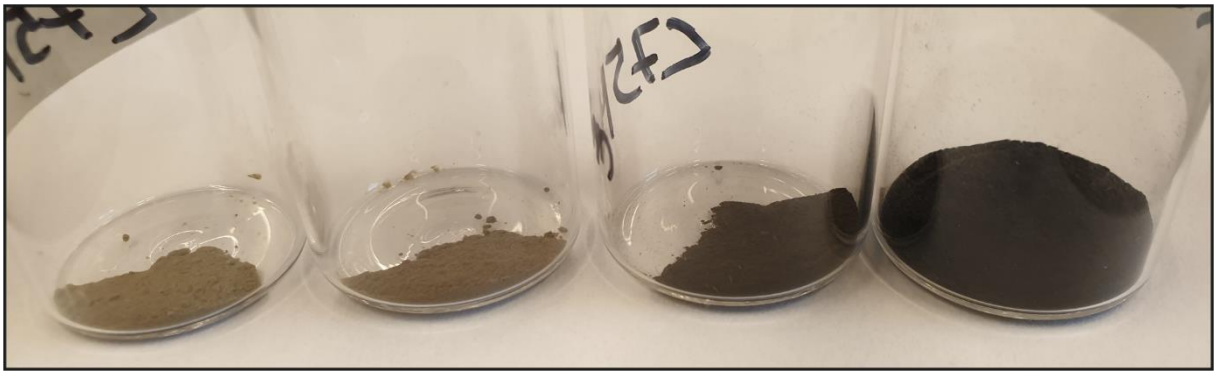

Figure 22 – Color differences between inactive (left pair) and active (right pair) catalysts. Catalysts from left to right: $Cu(NO_3)_2$/ACN; $Cu(NO_3)_2/H_2O$; $Cu(acac)_2$/ACN; co-impregnated. Catalysts shown are heat-treated and unreduced prior to catalysis. Inactive catalysts are distinctly a brighter color.

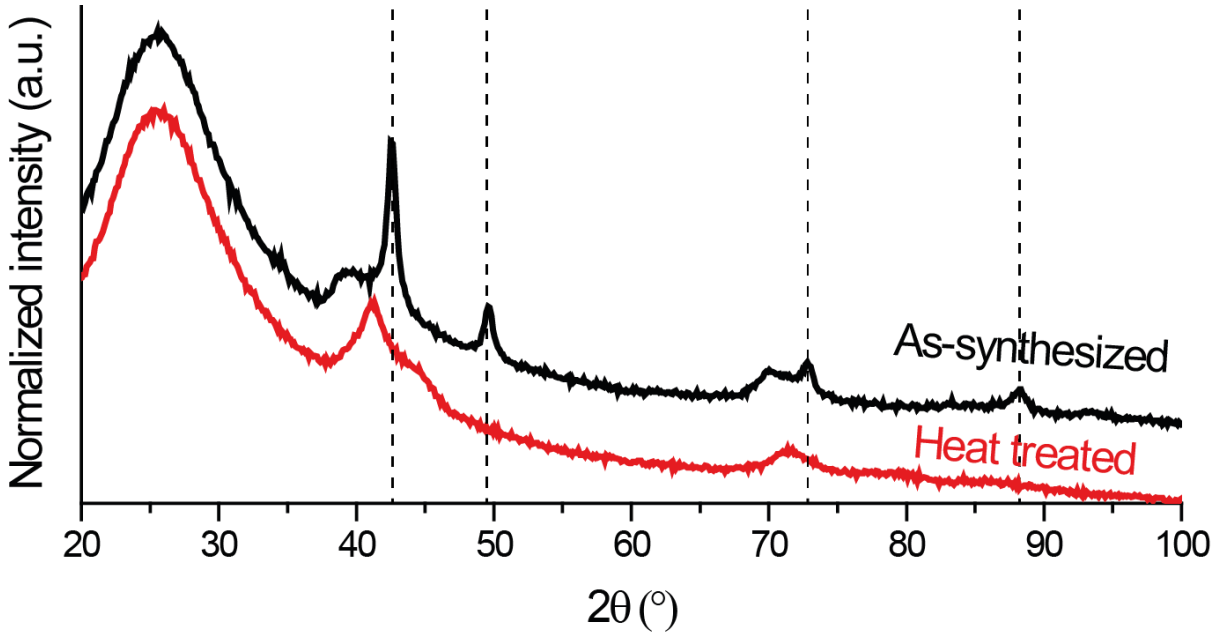

Figure 23 – X-ray diffractograms of a $CuCo/SiO_2$ catalyst as synthesized via galvanic replacement with $Cu(NO_3)_2/H_2O$ (black) and after heat treatment at 450 °C in synthetic air (red). The peaks belonging to $CoO/Cu_2O/Cu_{0.4}Co_{0.6}O$ are marked with a dashed line, and can be seen disappearing after heat treatment.

In Figure 23, the inactive catalyst $Cu(NO_3)_2/H_2O$ is shown before oxidation (in black) and after oxidation (in red), with the peaks from $CoO/Cu_2O/Cu_{0.4}Co_{0.6}O$ marked with dashed lines. After heat treatment, the sharp crystalline peaks have disappeared rather than forming Co_3O_4 as was seen before in Figure 14 (page 23). From the Scherrer equation, crystallite sizes of 14 nm were obtained prior to oxidation, while after oxidation the crystallite size is only 5 nm.

To complement the XRD data, catalyst $Cu(NO_3)_2/H_2O$ has been studied with electron microscopy as seen in Figure 24. Based on the particles observed, there is no indication of agglomerates with this technique after heat treatment either. The reduction was performed in-situ and immediately followed by catalysis, so no analysis was performed directly after reduction. The spent catalysts were also studied with EM and is shown in Figure 24c. Sintered metal particles are indeed visible, however support particles with many smaller metal particles were also observed which can also be seen in SI figure 9. While sintering is a major cause of deactivation for CuCo catalysts[6], it does not explain why some catalysts are completely inactive.

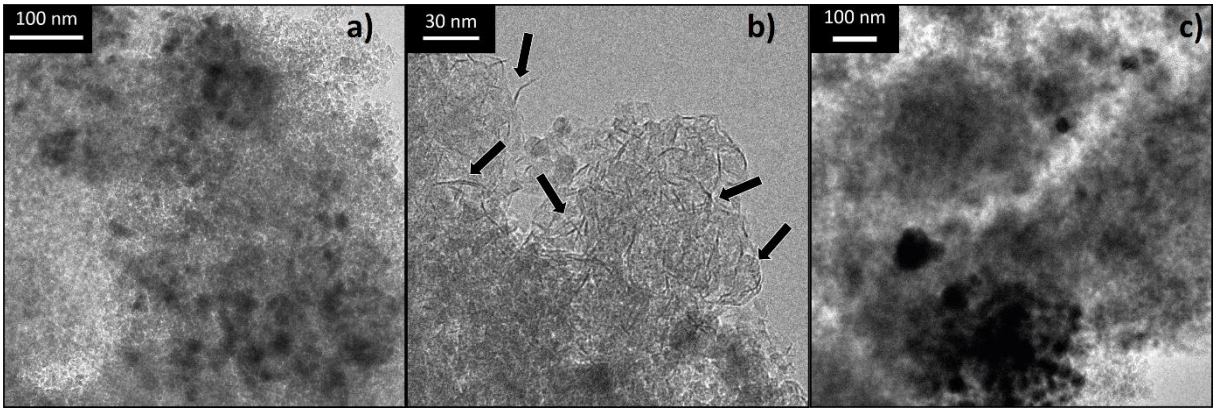

Figure 24 – BF-STEM images of $Cu(NO_3)_2/H_2O$ after oxidation (a, b), and after catalysis (c). Scale bars are 100, 30 and 100nm respectively. While metal particles clearly have sintered by comparing (a) to (c), smaller, clustered metal particles are still present as well (c). (b) shows 'spiked' features, some of which are indicated with arrows. These features were not observed prior to heat treatment.

Something peculiar was observed in the STEM images, however. Looking at the structure of $Cu(NO_3)_2/H_2O$ in Figure 24b (larger version is shown in SI figure 7), aside from the rounded silica support structure, there are also lines or 'spikes' visible. These features were not observed in the active catalysts nor in the supported cobalt particles prior to galvanic replacement. The 'spikes' are most likely cobalt silicates[48], as any nitrate would be removed during washing or decomposed during the following calcination/heat treatment[49] and copper species appear to have formed distinct Cu particles after heat treatment, though these were not visible in XRD. Cobalt silicates are known inactive species of Co/SiO_2 catalysts for FTS[50] and is an 'irreducible' species with a reduction temperature in excess of 600°C,[43] which is higher than the *in-situ* reduction temperature of 450°C used prior to catalysis. In order to test this hypothesis, a TPR measurement was performed on the inactive catalyst $Cu(NO_3)_2/H_2O$. The result can be seen in Figure 25. Compared to the prior TPR of CuCl/BTA, a sharp peak around 220°C has appeared and the peak around 450°C has disappeared. The peak at 220°C corresponds to the reduction of Cu (1)[51], while the peak at 710°C corresponds to the reduction of cobalt silicates (2)[43].

(1) $CuO + H_2 \rightarrow Cu + H_2O$

(2) $Co_2SiO_4 + 2\ H_2 \rightarrow 2\ Co + SiO_2 + 2\ H_2O$

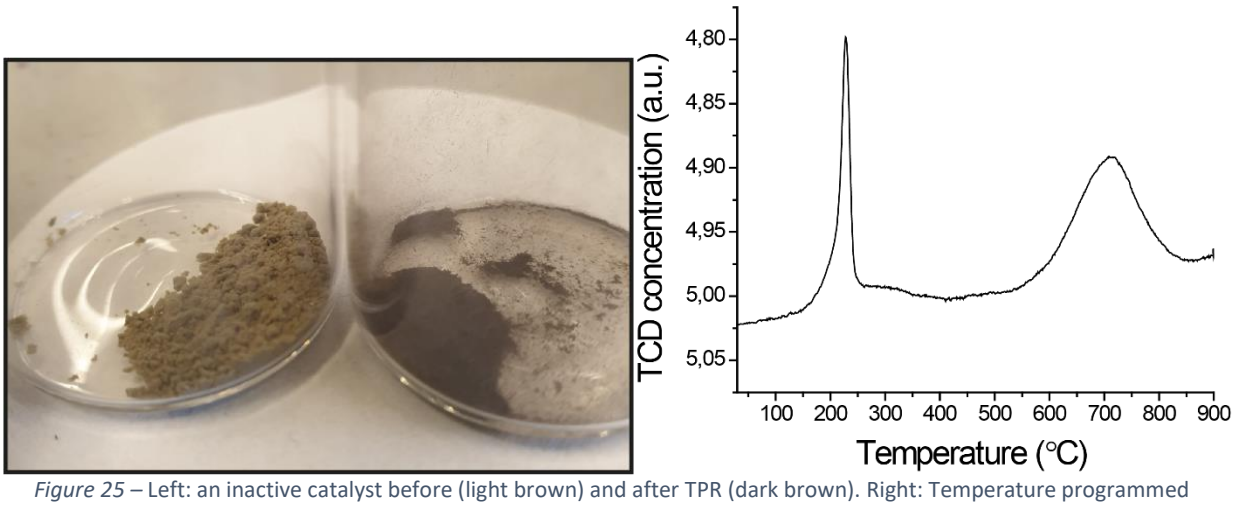

Figure 25 – Left: an inactive catalyst before (light brown) and after TPR (dark brown). Right: Temperature programmed reduction measurement of $Cu(NO_3)_2/H_2O$. The sharp peak around 220°C corresponds to the reduction of copper and the broad peak around 700°C the reduction of cobalt silicates.[43,51]

The sharp Cu peak compared to the TPR of CuCl/BTA (Figure 15) is likely due to the increased amount of Cu on this catalyst (3.33 wt% compared to 0.74wt%), and the absence of the peak around 450°C means that no cobalt oxides are present in the catalyst after heat treatment. Additionally, after TPR the reduced catalyst changed from its lighter brown colour to a very dark brown, similar to the active catalysts (Figure 25). Based on these observations, the inactivity of some catalysts is caused by the formation of cobalt silicates.

The next question is, why and how are these cobalt silicates formed? A paper by Haddad *et al.* goes into the effects of aqueous impregnation on prereduced and precalcined Co/SiO_2 catalysts.[43] One of their main conclusions is that drying of a "water impregnated", reduced and passivated Co/SiO_2 catalyst results in significant (hydro)silicate formation. The formation of the Co silicates is explained as a hydrothermal treatment during drying, where a drying temperature over 50°C would lead to significant amounts of Co silicates. They also noted an increase in Co dispersion after the formation of silicates, consistent with the observations made in Figure 11. As all three inactive catalysts were exposed to water at elevated temperatures while the active catalysts were not, the hydrothermal treatment explanation fits the experimental results very well.

5 Conclusions

One of the challenges to obtain better bimetallic CuCo catalysts for higher alcohol synthesis, is to obtain better intimacy between both metals. In prior work galvanic replacement (GR) was used on pre-deposited Co nanoparticles on SiO_2 with Cu ions to obtain bimetallic CuCo particles, however the amount of Cu deposited had been lower than aimed for. In this thesis the Cu deposition issue has been addressed by performing the galvanic replacement reaction on pre-deposited Co nanoparticles on SiO_2 with various Cu precursors and solvents.

First, three different batches of Co deposited on SiO_2 were prepared *via* incipient wetness impregnation as sacrificial templates for the galvanic replacement of Co with Cu. The galvanic replacement reaction was then successfully performed with various organic solvents, and Cu(I) and Cu(II) precursors. It was found that changing the organic solvent from long and apolar (oleylamine) to shorter and more polar (acetonitrile, *n*-butylamine) did not result in an improved quantity of Cu deposited on Co as determined by ICP. The ratio of Co removed from and Cu added to the catalyst was not according to the reaction stoichiometry of galvanic replacement either, excessive quantities of Co was removed from the catalysts in these cases. However, by changing from an organic to an aqueous Cu precursor solution, the galvanic replacement both followed the theoretical reaction stoichiometry and all Cu deposited from the precursor solution onto the catalyst. This result has shown that ideal galvanic replacement can be simply attained on pre-deposited Co nanoparticles on SiO_2 by choosing the correct solvent.

STEM-EDX was used to determine whether or not the Cu deposited selectively on top of Co after galvanic replacement. For the organic solvents, only oleylamine appeared to selectively deposit Cu on Co, while acetonitrile and *n*-butylamine seemingly deposited the Cu on both the support and Co. For the galvanic replacement with an aqueous solution, this could not be quantified due to the dispersion of metals likely induced by the drying steps used after synthesis. XRD experiments did not show any segregated (crystalline) Cu, suggesting a good intimacy between both metals after galvanic replacement.

The performance of the catalysts as prepared by galvanic replacement was compared to a catalyst as prepared by co-impregnation in the CO hydrogenation reaction. It was found that the GR catalysts had a lower selectivity towards methanol and a similar selectivity towards higher alcohols despite lower Cu/Co ratios, suggesting a better metal intimacy. In line with the work of Yang *et al.*[6], the selectivity towards long-chain products (both hydrocarbons and alcohols) decreases over time for these catalysts.

The catalysts prepared with aqueous Cu precursor solutions were inactive due to the formation of irreducible Co silicates, likely induced during drying, as determined by TPR. As using aqueous solutions is the most promising for the synthesis *via* galvanic replacement, future work should first focus on preventing the formation of these irreducible species.

6 Outlook

As the galvanic replacement with $Cu(II)(NO_3)_2$ in H_2O yielded the best results for synthesis, further research should be focussed on working with aqueous precursor solutions. There still are challenges to overcome to synthesize a CuCo catalyst via galvanic replacement properly. The first challenge is to prevent the formation of Co silicates which render the catalyst inactive due to the high temperature required to reduce those species. As the formation of silicates is suspected to be due to the presence of water near passivated cobalt at elevated temperatures, the simple solution would be to not expose the catalyst to elevated temperatures with water present. For the galvanic replacement reaction this should be no problem, as the reaction is driven by the difference in standard electrode potential. The drying could be done by washing a few times more in *e.g.* ethanol or acetone to remove as much water as possible and then leaving it to dry in air at room temperature. This should minimize the formation of Co silicates.

It was frequently challenging to precisely and accurately distinguish metal from support during particle size analysis by TEM (both BF and HAADF), which lead to usage of TEM mostly for qualitative observations. In order to facilitate statistical analysis, a support with a different texture/structure could be used, either a different silica-based support or something completely different like graphitic carbon.

Most information about the intimacy between both Cu and Co on the catalysts after synthesis was obtained from STEM-EDX maps, supplemented by XRD. While EDX allows for direct observation of both metals, it provides little detailed information about the exact structure. X-ray photoelectron spectroscopy could help with elucidating the bimetallic structure of these catalysts, as this surface-sensitive technique can be used to determine the surface molar metal ratios.[26]

Directly comparing the different catalysts synthesized by galvanic replacement to the one prepared by co-impregnation in the CO hydrogenation reaction was difficult, as there were many variables between the catalysts (*i.e.* metal loading, metal ratios, particle size, copper precursors). In order to compare the different synthesis methods better and to draw more convincing conclusions, the catalytic experiments need to be repeated with equal metal loadings, metal ratios and metal precursors. For example, comparing a catalyst prepared by co-impregnation of $Co(II)(NO_3)_2$ and $Cu(II)(NO_3)_2$ with a catalyst prepared by galvanic replacement of Co/SiO_2 (prepared from $Co(II)(NO_3)_2$) with an aqueous $Cu(II)(NO_3)_2$ solution. However, the aforementioned issue of Co silicate formation needs to be addressed first.

In one of the experiments, the sensitivity of the galvanic replacement to oxygen was tested. While it was clear that some oxygen was not detrimental to this reaction, the extent of the oxidation of Co was not determined prior to the reaction. In order to test if the reaction is fully insensitive to oxygen, galvanic replacement should be attempted with fully passivated Co/SiO_2, *i.e.* a CoO shell with a metallic Co core to test whether CoO would form a 'barrier' and protect the metallic Co from being replaced by Cu and how it would affect the structure.

7 Acknowledgements

First of all, I would like to thank professor Petra de Jongh for giving me the opportunity to do my master thesis in the Inorganic Chemistry and Catalysis group.

There are many people that helped me during the course of my research, who I would like to thank as well: Giorgio Totarella and Johan de Boed for general advice and assistance, Dennie Wezendonk for help with XRD and performing the TGA-MS experiments, Christa van Oversteeg, Lars van der Wal, Nynke Krans and Mark Meijerink for TEM imaging, Kang Cheng for H_2 chemisorption measurements, and anyone else who I might have forgotten to mention.

Furthermore, I'd like to thank my fellow students for helping me have a great time at ICC, especially Kristiaan Helferrich, Oscar Brandt Corstius and Andries van Hattem for interesting discussions and useful feedback.

And last but certainly not least, I'd like to deeply thank my daily supervisor Remco Dalebout for all his advice, feedback and assistance with many, many things, such as teaching me how to work in inert atmosphere. He was always enthusiastic, always made time for me whenever I had questions and always positive. He taught me a great many things and without a doubt made me a better scientist.

8 References

1. Angelici, C., Weckhuysen, B. M. & Bruijnincx, P. C. A. Chemocatalytic Conversion of Ethanol into Butadiene and Other Bulk Chemicals. *ChemSusChem* **6,** 1595–1614 (2013).

2. Luk, H. T., Mondelli, C., Ferré, D. C., Stewart, J. A. & Pérez-Ramírez, J. Status and prospects in higher alcohols synthesis from syngas. *Chem. Soc. Rev.* **46,** 1358–1426 (2017).

3. Nakagawa, Y., Tajima, N. & Hirao, K. A theoretical study of catalytic hydration reactions of ethylene. *J. Comput. Chem.* **21,** 1292–1304 (2000).

4. Bai, F. W., Anderson, W. A. & Moo-Young, M. Ethanol fermentation technologies from sugar and starch feedstocks. *Biotechnol. Adv.* **26,** 89–105 (2008).

5. Subramani, V. & Gangwal, S. K. A Review of Recent Literature to Search for an Efficient Catalytic Process for the Conversion of Syngas to Ethanol. *Energy & Fuels* **22,** 814–839 (2008).

6. Yang, Y. *et al.* Deactivation study of CuCo catalyst for higher alcohol synthesis via syngas. *Catal. Today* **270,** 101–107 (2016).

7. Forzatti, P., Tronconi, E. & Pasquon, I. Higher Alcohol Synthesis. *Catal. Rev.* **33,** 109–168 (1991).

8. Hu, J. *et al.* Conversion of biomass-derived syngas to alcohols and C2 oxygenates using supported Rh catalysts in a microchannel reactor. *Catal. Today* **120,** 90–95 (2007).

9. InfoMine - Mining Intelligence and Technology. Available at: http://www.infomine.com/. (Accessed: 6th March 2019)

10. Zaman, S. & Smith, K. J. A Review of Molybdenum Catalysts for Synthesis Gas Conversion to Alcohols: Catalysts, Mechanisms and Kinetics. *Catal. Rev.* **54,** 41–132 (2012).

11. Smith, K. J. & Anderson, R. B. The higher alcohol synthesis over promoted Cu/ZnO catalysts. *Can. J. Chem. Eng.* **61,** 40–45 (1983).

12. Frolich, K. & Cryder, D. S. Catalysts for the Formation of Alcohols from Carbon Monoxide and Hydrogen. *Ind. Eng. Chem.* **22,** 1051–1057 (1930).

13. Gupta, M., Smith, M. L. & Spivey, J. J. Heterogeneous catalytic conversion of dry syngas to ethanol and higher alcohols on Cu-based catalysts. *ACS Catalysis* **1,** 641–656 (2011).

14. Sugier, A. & Freund, E. Process for manufacturing alcohols and more particularly saturated linear primary alcohols from synthesis gas. 1–5 (1981).

15. Chaumette, P., Courty, P., Durand, D., Grandvallet, P. & Travers, C. Alcohol manufacturing process and catalyst therefor. (1985).

16. Xiaoding, X., Doesburg, E. B. M. & Scholten, J. J. F. Synthesis of higher alcohols from syngas - recently patented catalysts and tentative ideas on the mechanism. *Catal. Today* **2,** 125–170 (1987).

17. Matsuzaki, T., Takeuchi, K., Hanaoka, T. aki, Arawaka, H. & Sugi, Y. Effect of transition metals on oxygenates formation from syngas over Co/SiO2. *Appl. Catal. A, Gen.* **105,** 159–184 (1993).

18. Liu, G. *et al.* Nanoparticles of Cu-Co alloy supported on high surface area LaFeO3 - Preparation and catalytic performance for higher alcohol synthesis from syngas. *RSC Adv.* **5,** 31637–31647 (2015).

19. Nafria, R. *et al.* Co-Cu Nanoparticles: Synthesis by Galvanic Replacement and Phase

Rearrangement during Catalytic Activation. *Langmuir* **32,** 2267–2276 (2016).

20. Prieto, G. *et al.* Design and synthesis of copper-cobalt catalysts for the selective conversion of synthesis gas to ethanol and higher alcohols. *Angew. Chemie - Int. Ed.* **53,** 6397–6401 (2014).

21. Xiao, K. *et al.* CuFe, CuCo and CuNi nanoparticles as catalysts for higher alcohol synthesis from syngas: A comparative study. *Catal. Sci. Technol.* **3,** 1591–1602 (2013).

22. Xiao, K. *et al.* Advances in bifunctional catalysis for higher alcohol synthesis from syngas. *Chinese J. Catal.* **34,** 116–129 (2013).

23. Xia, X., Wang, Y., Ruditskiy, A. & Xia, Y. 25th Anniversary Article: Galvanic Replacement: A Simple and Versatile Route to Hollow Nanostructures with Tunable and Well-Controlled Properties. *Adv. Mater.* **25,** 6313–6333 (2013).

24. Mallory, G. O., Hajdu, J. B. & American Electroplaters and Surface Finishers Society. *Electroless plating : fundamentals and applications*. (The Society, 1990).

25. Djokić, S. S. & Cavallotti, P. L. Electroless Deposition: Theory and Applications. in 251–289 (Springer, New York, NY, 2010). doi:10.1007/978-1-4419-5589-0_6

26. Zhou, G., Dong, Y. & He, D. Bimetallic Ru–M/TiO2 (M = Fe, Ni, Cu, Co) nanocomposite catalysts facribated by galvanic replacement: Structural elucidation and catalytic behavior in benzene selective hydrogenation. *Appl. Surf. Sci.* **456,** 1004–1013 (2018).

27. Herremans, B. & Dalebout, R. Synthesis of supported CuCo-based catalysts via galvanic replacement for CO hydrogenation towards higher oxygenates. (2017).

28. G. Leendert Bezemer *et al.* Cobalt Particle Size Effects in the Fischer−Tropsch Reaction Studied with Carbon Nanofiber Supported Catalysts. (2006). doi:10.1021/JA058282W

29. Günter, M. M. *et al.* Implication of the microstructure of binary Cu/ZnO catalysts for their catalytic activity in methanol synthesis. *Catal. Letters* **71,** 37–44 (2001).

30. Baker, J. E., Burch, R., Hibble, S. J. & Loader, P. K. Properties of silica-supported Cu/Co bimetallic catalysts in the synthesis of higher alcohols. *Appl. Catal.* **65,** 281–292 (1990).

31. Smith, M. L., Kumar, N. & Spivey, J. J. CO Adsorption Behavior of Cu/SiO_2, Co/SiO_2, and $CuCo/SiO_2$ Catalysts Studied by in Situ DRIFTS. *J. Phys. Chem. C* **116,** 7931–7939 (2012).

32. Chorkendorff, I. & Niemantsverdriet, J. W. *Concepts of Modern Catalysis and Kinetics*. (2003).

33. Da Silva, A. G. M., Rodrigues, T. S., Haigh, S. J. & Camargo, P. H. C. Galvanic replacement reaction: Recent developments for engineering metal nanostructures towards catalytic applications. *Chemical Communications* **53,** 7135–7148 (2017).

34. Gilroy, K. D., Farzinpour, P., Sundar, A., Hughes, R. A. & Neretina, S. Sacrificial templates for galvanic replacement reactions: Design criteria for the synthesis of pure pt nanoshells with a smooth surface morphology. *Chem. Mater.* **26,** 3340–3347 (2014).

35. You, L., Mao, Y. & Ge, J. Synthesis of stable SiO2@Au-nanoring colloids as recyclable catalysts: Galvanic replacement taking place on the surface. *J. Phys. Chem. C* **116,** 10753–10759 (2012).

36. Mintsouli, I. *et al.* Pt-Cu electrocatalysts for methanol oxidation prepared by partial galvanic replacement of Cu/carbon powder precursors. *Appl. Catal. B Environ.* **136–137,** 160–167 (2013).

37. Chen, J. *et al.* Facile synthesis of gold-silver nanocages with controllable pores on the surface. *J. Am. Chem. Soc.* **128,** 14776–14777 (2006).

38. Cobley, C. M., Zhang, Q., Song, W. & Xia, Y. The Role of Surface Nonuniformity in Controlling the Initiation of a Galvanic Replacement Reaction. *Chem. - An Asian J.* **6,** 1479–1484 (2011).

39. Vanýsek, P. CRC Handbook of Chemistry and Physics, 92th Edition.

40. Greeley, J. & Nørskov, J. K. Electrochemical dissolution of surface alloys in acids: Thermodynamic trends from first-principles calculations. *Electrochim. Acta* **52,** 5829–5836 (2007).

41. De Jong, K. P. *Synthesis of Solid Catalysts*. *Synthesis of Solid Catalysts* (Wiley-VCH, 2009). doi:10.1002/9783527626854

42. Patterson, A. L. The Scherrer Formula for X-Ray Particle Size Determination. *Phys. Rev.* **56,** 978–982 (1939).

43. Haddad, G. J. & Goodwin, J. G. The impact of aqueous impregnation on the properties of prereduced vs precalcined Co/SiO2. *J. Catal.* **157,** 25–34 (1995).

44. PDF-4+ 2018, International Centre for Diffraction Data, database version 4.1801.

45. Smith, M. L., Campos, A. & Spivey, J. J. Reduction processes in Cu/SiO 2, Co/SiO 2, and CuCo/SiO 2 catalysts. in *Catalysis Today* **182,** 60–66 (Elsevier, 2012).

46. Riva, R., Miessner, H., Vitali, R. & Del Piero, G. Metal–support interaction in Co/SiO2 and Co/TiO2. *Appl. Catal. A Gen.* **196,** 111–123 (2000).

47. Wang, J., Chernavskii, P. A., Khodakov, A. Y. & Wang, Y. Structure and catalytic performance of alumina-supported copper–cobalt catalysts for carbon monoxide hydrogenation. *J. Catal.* **286,** 51–61 (2012).

48. Kiss, G., Kliewer, C. E., DeMartin, G. J., Culross, C. C. & Baumgartner, J. E. Hydrothermal deactivation of silica-supported cobalt catalysts in Fischer-Tropsch synthesis. *J. Catal.* **217,** 127–140 (2003).

49. Małecka, B., Łącz, A., Drozdz, E. & Małecki, A. Thermal decomposition of d-metal nitrates supported on alumina. *J. Therm. Anal. Calorim.* **119,** 1053–1061 (2015).

50. Kababji, A. H., Joseph, A. B. & Wolan, A. J. T. Silica-Supported Cobalt Catalysts for Fischer-Tropsch Synthesis: Effects of Calcination Temperature and Support Surface Area on Cobalt Silicate Formation. doi:10.1007/s10562-009-9903-4

51. Chen, C. S., Cheng, W. H. & Lin, S. S. Study of reverse water gas shift reaction by TPD, TPR and CO2 hydrogenation over potassium-promoted Cu/SiO2catalyst. *Appl. Catal. A Gen.* **238,** 55–67 (2002).

9 Supplementary information

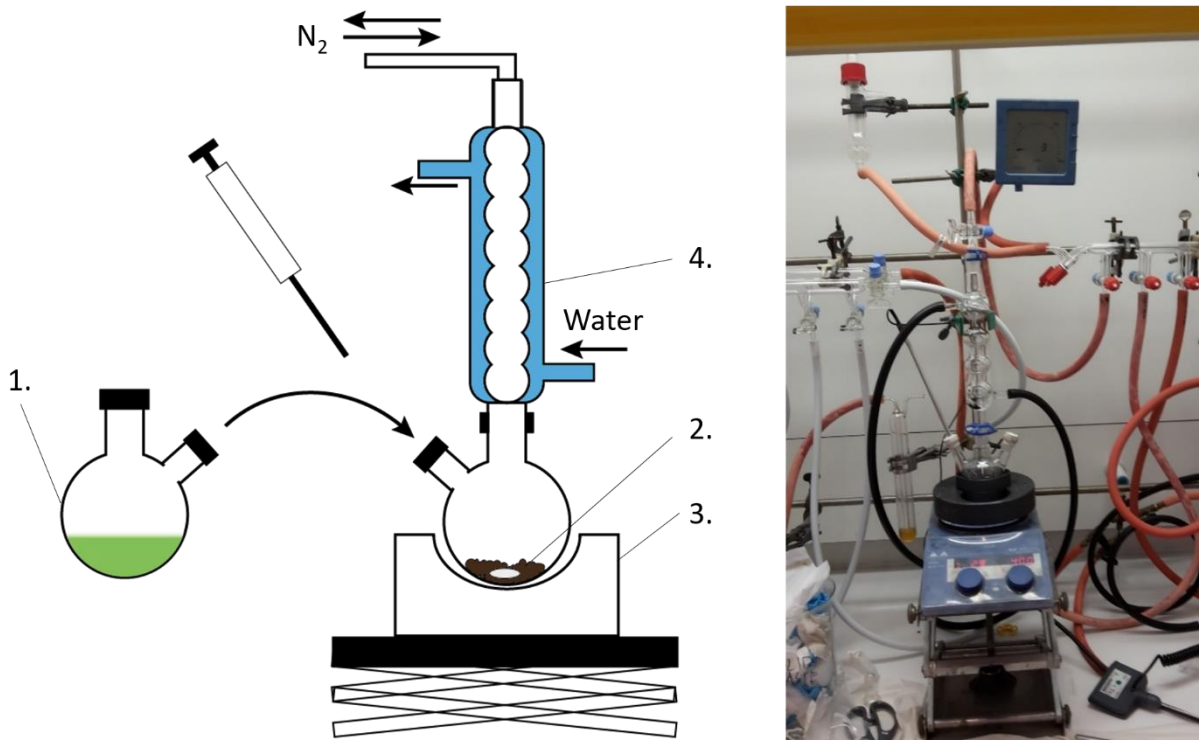

SI figure 1 – Schematic representation of the GR setup (left) and the real setup (right). The numbered items are as follows: (1) Oxygen- and water-free $Cu^{(2)+}$ solution in an inert atmosphere. (2) Flask loaded with Co/SiO_2 and a magnetic stirrer in inert atmosphere. (3) Heating mantle and stirring plate. (4) Water-cooled condenser to prevent solvent evaporation.

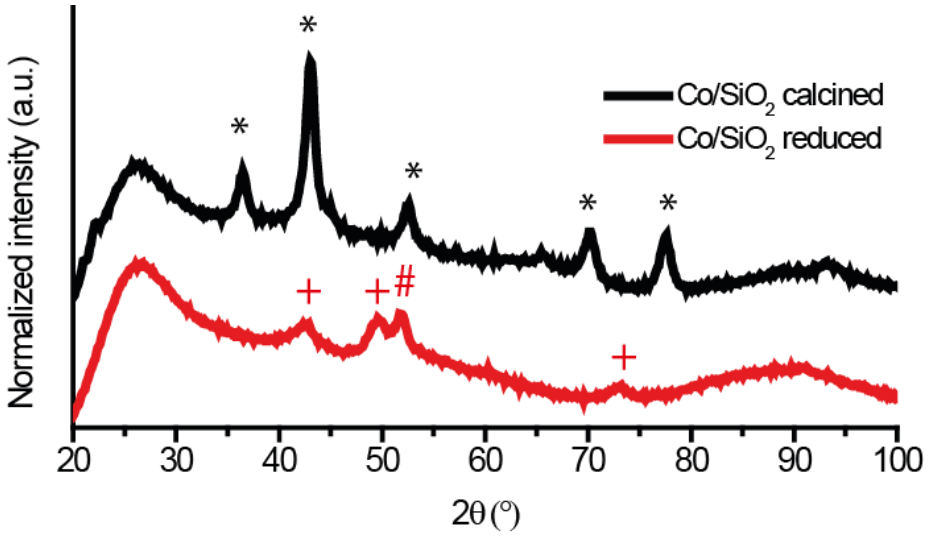

SI figure 2 – Diffractograms of a Co/SiO_2 template after impregnation and calcination (black) and reduction (red). * corresponds to Co_3O_4, + to CoO and # to metallic Co. CoO is present in the reduced sample due to the used equipment for diffraction experiments not being completely airtight, leading to partial oxidation of the metallic Co present.

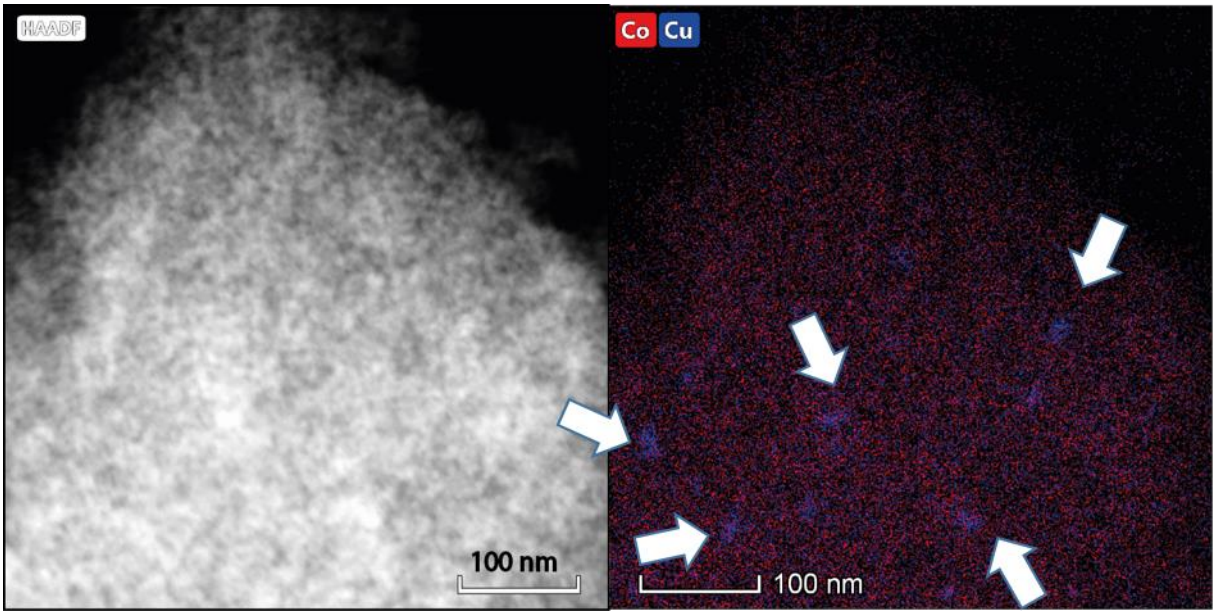

SI figure 3 – STEM-EDX map of $Cu(NO_3)_2/H_2O$, showing the HAADF-STEM image (left), and the Cu (blue) and Co (red) EDX map overlapped (right). Several distinct Cu particles of around 20 nm are visible in the EDX map, several are indicated with white arrows. Observing particles like these was the exception rather than the norm.

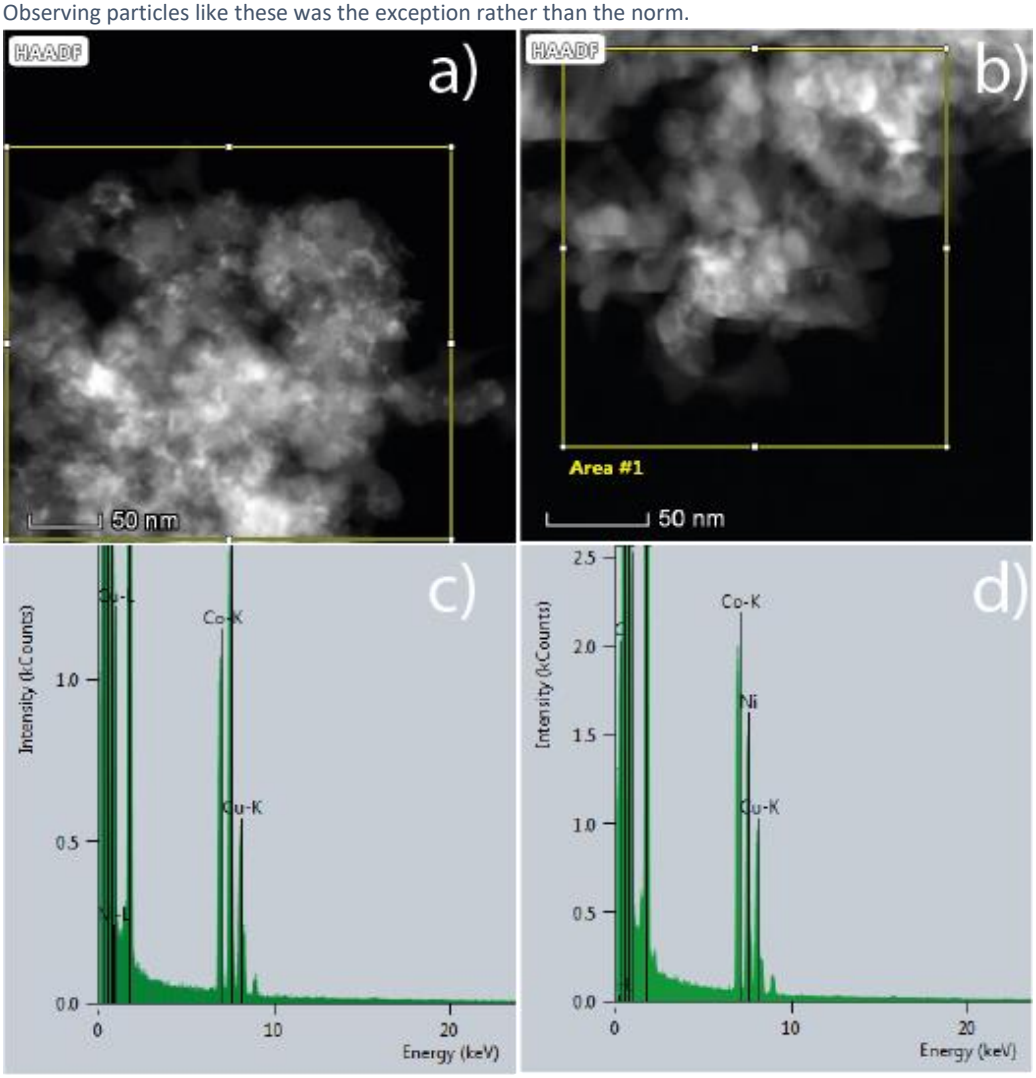

SI figure 4 – HAADF-STEM images of the co-impregnated catalyst (a, b) and their respective EDX spectra (c, d). The peak relative intensity of Co-K and Cu-K are roughly constant. The Ni peak is due to the Ni grid of the sample.

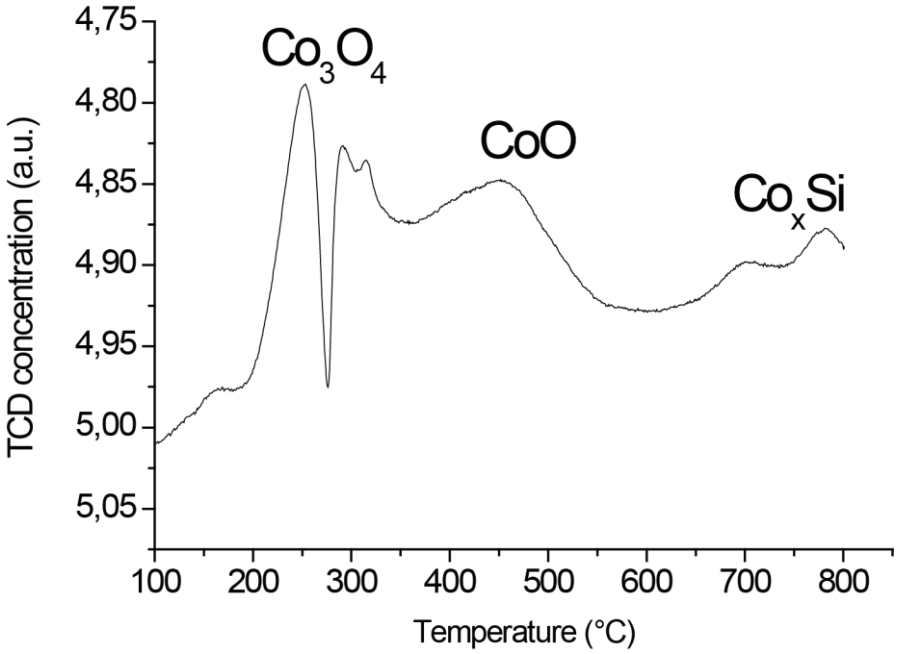

SI figure 6 – TPR of batch 1 of Co/SiO_2 after calcination. 450 °C is used as the reduction temperature based on this TPR profile. The peaks are attributed to Co_3O_4, CoO and Co silicates respectively.[43,46] Around 300 °C a sharp decrease immediately followed by a sharp increase is visible, this is attributed to instrumental error.

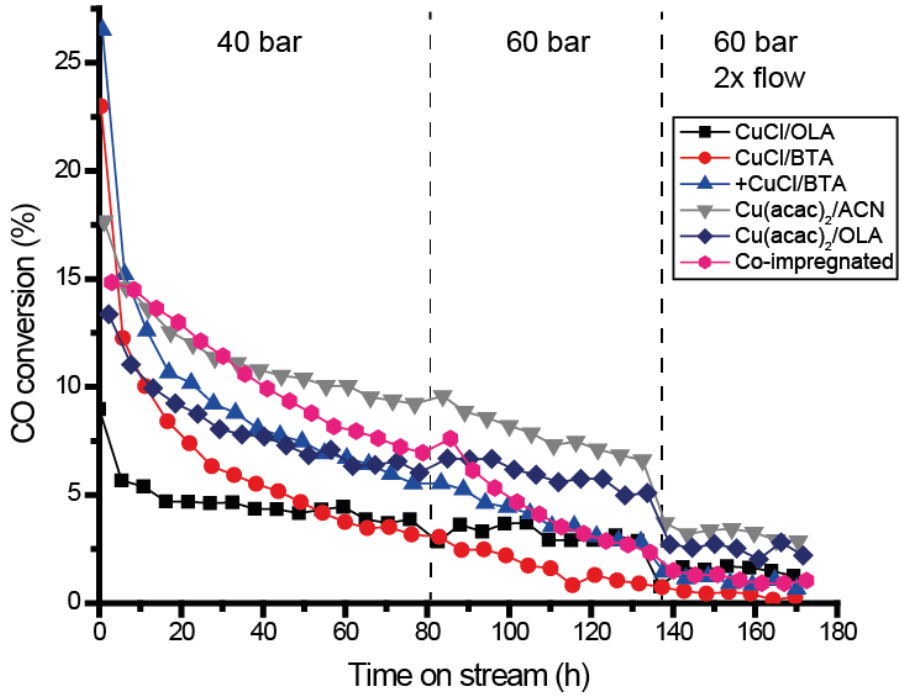

SI figure 5 – CO conversion (%) of the $CuCo/SiO_2$ catalysts plotted against the time on stream – H_2/CO = 2/1 V/V, P = 40 bar (left region); 60 bar (center and right), GHSV = 820-5000 h^{-1}, T = 250°C. The gas flow is doubled in the third region.

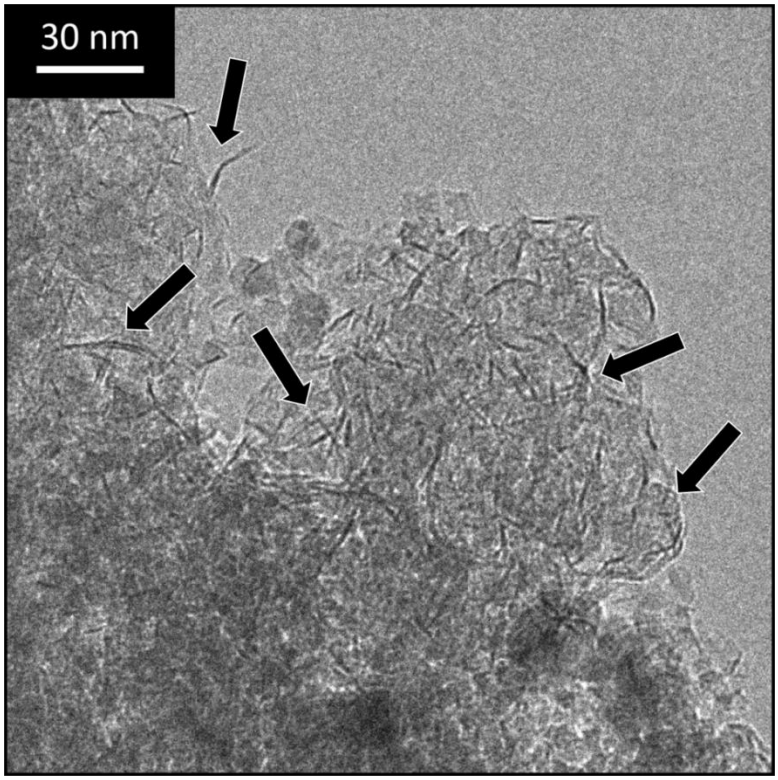

SI figure 7 – BF-STEM image of $Cu(NO_3)_2/H_2O$ after oxidation. 'Spiked' features are visible, some of which are indicated with arrows. These features were not observed prior to heat treatment, and are suspected to be cobalt silicates.

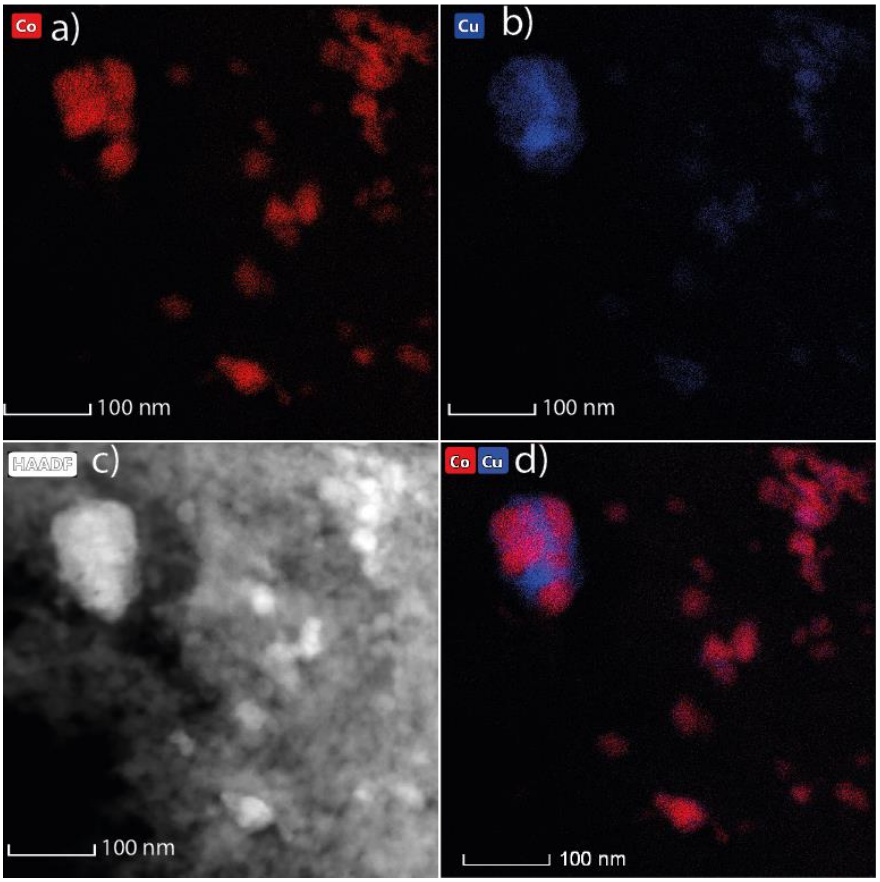

SI figure 8 – STEM-EDX map of CuCl/OLA after catalysis, showing STEM-EDX of Co (a), Cu overlapped (b), and the HAADF-STEM (c) and Co,Cu overlapped (d). Large, sintered and dealloyed particles have clearly formed as can be seen in these images.

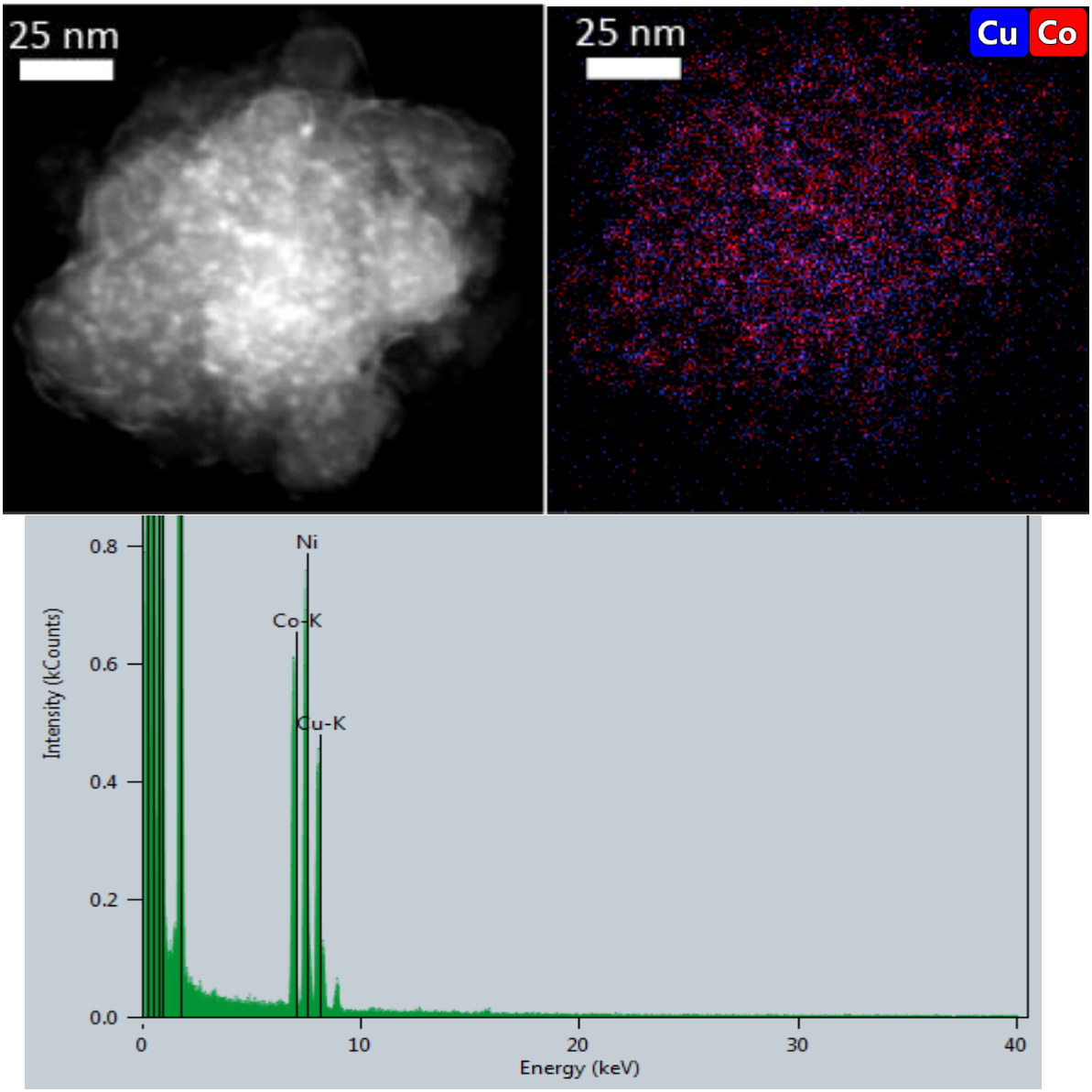

SI figure 9 – HAADF-STEM image and EDX map of a single spent catalyst particle of $Cu(NO_3)_2/H_2O$, with the EDX spectrum shown underneath. Small and dispersed metal particles are visible in the STEM image, which appear to be mixed metals according to the EDX map with comparable intensities. The Ni peak in the EDX spectrum is due to the deposition of the sample on a Ni grid.